Extensive Regulatory Changes in Genes Affecting Vocal and Facial Anatomy Separate Modern from Archaic Humans

David Gokhman[1], Lily Agranat-Tamir[1,2], Genevieve Housman[3,4], Raquel García-Pérez[5], Malka Nissim-Rafinia[1], Swapan Mallick[6,7,8], Maria A. Nieves-Colón[3,4], Heng Li[6], Songül Alpaslan-Roodenberg[7], Mario Novak[9,22], Hongcang Gu[6], Manuel Ferrando-Bernal[5], Pere Gelabert[5], Iddi Lipende[10], Ivanela Kondova[11], Ronald Bontrop[11], Ellen E. Quillen[12], Alexander Meissner[6,13,14], Anne C. Stone[3,4,15], Anne E. Pusey[16], Deus Mjungu[10], Leonid Kandel[17], Meir Liebergall[17], María E. Prada[18], Julio M. Vidal[19], Kay Prüfer[20], Johannes Krause[21], Benjamin Yakir[2], Svante Pääbo[20], Ron Pinhasi[22,23], Carles Lalueza-Fox[5], David Reich[6,7,8], Tomas Marques-Bonet[5,24,25], Eran Meshorer[1,26,*], Liran Carmel[1,*]

[1] Department of Genetics, The Alexander Silberman Institute of Life Sciences, Faculty of Science, The Hebrew University of Jerusalem, Edmond J. Safra Campus, Givat Ram, Jerusalem 91904, Israel.
[2] Department of Statistics, The Hebrew University of Jerusalem, Jerusalem 91905, Israel.
[3] School of Human Evolution and Social Change, Arizona State University, Tempe, AZ 85281, USA.
[4] Center for Evolution and Medicine, Arizona State University, Tempe, AZ 85287, USA.
[5] Institute of Evolutionary Biology (UPF-CSIC), 08003 Barcelona, Spain.
[6] Broad Institute, Cambridge MA 02138, USA.
[7] Department of Genetics, Harvard Medical School, Boston, MA 02115, USA.
[8] Howard Hughes Medical Institute, Harvard Medical School, Boston, MA 02115, USA.
[9] Institute for Anthropological Research, Ljudevita Gaja 32, 10000 Zagreb, Croatia.
[10] Gombe Stream Research Center, Jane Goodall Institute, Kigoma, Tanzania.
[11] Biomedical Primate Research Center (BPRC), Rijswijk, The Netherlands.
[12] Department of Genetics, Texas Biomedical Research Institute, San Antonio, Texas 85287, USA.
[13] Harvard Stem Cell Institute, Cambridge, MA 02138 USA.

[14] Department of Stem Cell and Regenerative Biology, Harvard University, Cambridge, MA 02138 USA
[15] Institute of Human Origins, Arizona State University, Tempe, AZ 85287, USA.
[16] Department of Evolutionary Anthropology , Duke University , Durham, NC 27708, USA.
[17] Orthopaedic Department, Hadassah – Hebrew University Medical Center, Jerusalem, Israel.
[18] I.E.S.O. 'Los Salados'. Junta de Castilla y León, Spain.
[19] Junta de Castilla y León, Servicio de Cultura de León, Spain.
[20] Department of Evolutionary Genetics, Max Planck Institute for Evolutionary Anthropology, Leipzig D-04103, Germany.
[21] Max Planck Institute for the Science of Human History, 07745 Jena, Germany.
[22] Earth Institute and School of Archaeology, University College Dublin, Dublin 4, Ireland.
[23] Department of Anthropology, University of Vienna, Althanstrasse 14, 1090, Vienna, Austria.
[24] Catalan Institution of Research and Advanced Studies (ICREA), 08010 Barcelona, Spain.
[25] Centro Nacional de Análisis Genómico (CRG-CNAG), 08028 Barcelona, Spain.
[26] The Edmond and Lily Safra Center for Brain Sciences (ELSC), The Hebrew University of Jerusalem, Edmond J. Safra Campus, Givat Ram, Jerusalem, 91904, Israel.

Lead Contact: Liran Carmel (liran.carmel@huji.ac.il)

Summary

Changes in gene regulation are broadly accepted as key drivers of phenotypic differences between closely related species. However, identifying regulatory changes that shaped human-specific traits is a challenging task. Here, we use >60 DNA methylation maps of ancient and present-day human groups, as well as six chimpanzees, to detect regulatory changes that emerged in modern humans after the split from Neanderthals and Denisovans. We show that genes affecting vocalization and facial features went through particularly extensive methylation changes. Specifically, we identify silencing patterns in a network of genes (*SOX9*, *ACAN*, *COL2A1* and *NFIX*), and propose that they might have played a role in the reshaping of human facial morphology, and in forming the 1:1 vocal tract configuration that is considered optimal for speech. Our results provide insights into the molecular mechanisms that might underlie vocal and facial evolution, and suggest that they arose after the split from Neanderthals and Denisovans.

Keywords: Epigenetics, Paleoepigenetics, aDNA, Neandertal, Denisova, Gene regulation, Craniofacial morphology, larynx, vocal cords, voice box

Introduction

The advent of high-quality ancient genomes of archaic humans (Neanderthal and Denisovan) opened up the possibility to identify the genetic basis of some unique modern human traits (Meyer et al., 2012; Prüfer et al., 2014). A common approach is to carry out sequence comparisons and detect non-neutral sequence changes. However, out of ~30,000 substitutions and indels that reached fixation on the lineage of present-day humans after their separation from archaic humans, only ~100 directly alter amino acid sequence (Prüfer et al., 2014), and currently, our ability to estimate the biological effects of the remaining ~30,000 changes is very restricted. Although most of these noncoding changes are probably nearly neutral, many others may affect gene function, especially those in regulatory regions like promoters and enhancers. Such regulatory changes may have sizeable impact on human evolution, as alterations in gene regulation are thought to underlie much of the phenotypic variation between closely related groups (Fraser, 2013; King and Wilson, 1975). Thus, examining directly DNA regulatory layers such as DNA methylation could enhance our understanding of the development of human-specific traits far beyond what can be achieved using sequence comparison alone (Hernando-Herraez et al., 2015a).

In order to gain insight into the regulatory changes that underlie human evolution, we previously developed a method to reconstruct antemortem DNA methylation maps of ancient genomes (Gokhman et al., 2014) based on analysis of patterns of damage to ancient DNA (Briggs et al., 2010; Gokhman et al., 2014; Pedersen et al., 2014). We applied this method to reconstruct the methylomes of a Neanderthal and a Denisovan, which were then compared to a present-day osteoblast methylation map. However, the ability to identify differentially methylated regions (DMRs) between the human groups was confined by the incomplete osteoblast reference map

(providing methylation information for ~10% of CpG sites), differences in sequencing technologies, lack of an outgroup and a restricted set of skeletal samples (see Methods). To study the evolutionary dynamics of DNA methylation along the hominin tree on a larger scale, we establish here a comprehensive assembly of skeletal DNA methylation maps from modern humans, archaic humans, and chimpanzees. We then integrate these data with known anatomical effects of genes (Gokhman et al., 2017a; Köhler et al., 2014), and find that genes that affect vocal, facial, and pelvic anatomy have gone through extensive DNA methylation changes that are unique to modern humans.

Results

We reconstructed ancient DNA methylation maps of eight individuals: in addition to the previously published Denisovan and Altai Neanderthal methylation maps (Gokhman et al., 2014), we reconstructed the methylome of the Vindija Neanderthal (~40,000 years before present, ybp), and three methylomes of anatomically modern humans: the Ust'-Ishim individual (~45,000 ybp) (Fu et al., 2014), the Loschbour individual (~8,000 ybp) (Lazaridis et al., 2014), and the Stuttgart individual (~7,000 ybp) (Lazaridis et al., 2014). We also sequenced to high-coverage and reconstructed the methylomes of the La Braña 1 individual (~8,000 ybp, 22x) (which was previously sequenced to low-coverage (Olalde et al., 2014) and an individual from Anatolia, Turkey (I1583, 24x, ~8,500 ybp), which was previously sequenced using a capture array (Mathieson et al., 2015).

To this we added 52 publicly available partial bone methylation maps from present-day individuals, produced using 450K methylation arrays (Horvath et al., 2015; Lokk et al., 2014). To obtain full present-day bone maps, we produced whole-genome bisulfite sequencing (WGBS)

methylomes from the femur bones of two individuals (Bone1 and Bone2). Hereinafter, ancient and present-day modern humans are collectively referred to as *modern humans* (MHs), while the Neanderthal and Denisovan are referred to as *archaic humans*. As an outgroup, we produced methylomes of five chimpanzees (one WGBS and four 850K methylation arrays). Together, these data establish a unique and comprehensive platform to study DNA methylation dynamics in recent human evolution (Table S1).

Identification of DMRs

Methylation maps may differ due to factors such as sex, age, health, environment, and tissue type. In addition, the comparison of DNA methylation maps that were produced using different technologies could potentially introduce artifacts in DMR-detection. In order to account for these confounding factors and to identify DMRs that reflect evolutionary differences between human groups, we took a series of steps. To minimize false positives that could arise from the comparison of maps produced using various technologies, we set the reconstructed Ust'-Ishim methylome as the MH reference, to which we compared the Altai Neanderthal and the Denisovan. We developed a DMR-detection method for ancient methylomes, which accounts for potential noise introduced during reconstruction, as well as differences in coverage and deamination rates (Figure 1 and Methods). To minimize the number of false positives and to identify DMRs that are most likely to have a regulatory effect, we applied a strict threshold of >50% difference in methylation across a minimum of 50 CpGs. This also filters out environmentally-induced DMRs which typically show low methylation differences and limited spatial scope (Gokhman et al., 2017b). Using this method, we identified 9,679 regions that showed methylation differences between these individuals. These regions do not necessarily represent evolutionary differences between the human groups. Rather, many of them could be attributed to factors separating the three individuals (e.g., Ust'-Ishim is a

male whereas the archaic humans are females), or to variability within populations. To minimize such effects, we used the 59 additional human maps to filter out regions where variability in methylation is detected. We adopted a conservative approach, whereby we take only loci where methylation in one hominin group is found completely outside the range of methylation in the other groups. Importantly, our samples come from both sexes, from individuals of various ages and ancestries, from sick and healthy individuals, and from a variety of skeletal parts (femur, skull, phalanx, tooth, and rib; Table S1). Hence, the use of these samples to filter out DMRs is expected to cover much of the variation that stems from the above factors (Figure 1, Figure 2A-C). This step resulted in a set of 7,649 DMRs that discriminate between the human groups, which we ranked according to their significance level.

Next, using the chimpanzee samples, we were able to determine for 2,825 of these DMRs the lineage where the methylation change occurred (Figures 2D and 3A). Of these DMRs 873 are MH-derived, 939 are archaic-derived, 443 are Denisovan-derived, and 570 are Neanderthal-derived (Figure 3A, Table S2). The extensive set of MH maps used to filter out within-population variability led us to focus in this work on MH-derived DMRs.

Face and voice-affecting genes are derived in MHs

We defined differentially methylated genes (DMGs) as genes that overlap at least one DMR along their body or up to a distance of 5 kb upstream. The 873 MH-derived DMRs are linked to 588 MH-derived DMGs (Table S2). To gain insight into the function of these DMGs, we first analyzed their gene ontology (GO). As expected from a comparison between skeletal tissues, MH-derived DMGs are enriched with terms associated with the skeleton (e.g., *endochondral bone morphogenesis, trabecula morphogenesis, palate development, regulation of cartilage*

development, chondrocyte differentiation and bone morphogenesis). Also notable are terms associated with the skeletal muscle, cardiovascular, and nervous system (Table S3).

To acquire a more precise understanding of the possible functional consequences of these DMGs, we used Gene ORGANizer, which links human genes to the organs they phenotypically affect (Gokhman et al., 2017a). Unlike tools that use GO terms or RNA expression data, Gene ORGANizer is based entirely on curated gene-disease and gene-phenotype associations from monogenic diseases. Therefore, it relies on direct phenotypic observations in human patients whose condition results from known gene perturbations. Using Gene ORGANizer we found 11 organs that are over-represented within the 588 MH-derived DMGs, eight of which are skeletal parts that can be divided into three regions: the voice box (larynx), face, and pelvis (Figure 3B, Table S4). The strongest enrichment was observed in the laryngeal region (x2.11 and x1.68, FDR = 0.017 and 0.048, for the vocal cords and larynx, respectively), followed by facial and pelvic structures, including the teeth, forehead, jaws, and pelvis. Interestingly, the face and pelvis are considered the most morphologically divergent regions between Neanderthals and MHs (Weaver, 2009) and our results reflect this divergence through gene regulation changes. The enrichment of the vocal tract (the pharyngeal, oral, and nasal cavities, where sound is filtered to specific frequencies) (Fitch, 2000; Lieberman, 2007) is also apparent when examining patterns of gene expression. This analysis shows that the pharynx and larynx are the most enriched organs within MH-derived DMGs (1.7x and 1.6x, FDR = 5.6×10^{-6} and FDR = 7.3×10^{-7}, respectively, Table S3). We also found that 29 of the MH-derived DMRs overlap previously reported craniofacial development enhancers (4.97-fold compared to expected, $P < 10^{-6}$, randomization test) (Prescott et al., 2015).

To test whether this enrichment remains if we take only the most confident DMRs, we limited the analysis only to DMGs where the most significant DMRs are found (top quartile). Here, the over-representation of voice-affecting genes is more pronounced, with the vocal cords enriched almost 3-fold (FDR = 0.028), and the larynx over 2-fold (FDR = 0.028, Figure 3C, Table S4).

Next, we hypothesized that skeletal-associated genes are likely to be enriched when comparing DNA methylation maps originating from bones, hence introducing potential biases. To test whether the over-representation of the larynx, face, and pelvis is a consequence of this, we compared the fraction of genes affecting the face, larynx, and pelvis among all skeletal genes to their fraction within the skeletal genes in the MH-derived DMGs. We found that genes affecting the face, larynx, and pelvis are significantly over-represented within skeletal MH-derived DMGs ($P = 1.0 \times 10^{-5}$, $P = 1.3 \times 10^{-3}$, $P = 2.1 \times 10^{-3}$, P = 0.03, for vocal cords, larynx, face, and pelvis, respectively, hypergeometric test). Additionally, we conducted a permutation test on the list of 129 MH-derived DMGs that are linked to organs on Gene ORGANizer, replacing those that are linked to the skeleton with randomly selected skeletal-related genes. We then ran the list in Gene ORGANizer and computed the enrichment. We repeated the process 100,000 times and found that the enrichment levels we observed within MH-derived DMGs are significantly higher than expected by chance for the laryngeal and facial regions, but not for the pelvis ($P = 8.6 \times 10^{-6}$, $P = 6.6 \times 10^{-4}$, $P = 4.3 \times 10^{-5}$, and $P = 6.5 \times 10^{-3}$, for vocal cords, larynx, face and pelvis, respectively, Figure S1A). Thus, the fact that the DMGs were detected in a comparison of bone methylomes is unlikely to underlie the observed enrichment of the larynx, vocal cords, and face, but it could potentially drive the enrichment of genes related to the pelvis. We therefore focus hereinafter on genes affecting the facial and laryngeal regions.

We next analyzed whether pleiotropy could underlie the observed enrichments. To some extent, Gene ORGANizer negates pleiotropic effects (Gokhman et al., 2017a). Despite the fact that the DMGs belong to different pathways, and some have pleiotropic functions (Gokhman et al., 2017a; Kanehisa et al., 2016; Köhler et al., 2014), their most significantly shared properties are still in shaping the vocal and facial anatomy. Nevertheless, we tested this possibility more directly, estimating the pleiotropy of each gene by counting the number of different Human Phenotype Ontology (HPO) terms that are associated with it across the entire body (Köhler et al., 2014). We found that DMGs do not tend to be more pleiotropic than the rest of the genome ($P = 0.17$, *t*-test), nor do voice- and face-affecting DMGs tend to be more pleiotropic than other DMGs ($P = 0.19$ and $P = 0.27$, respectively).

Potentially, longer genes have higher probability to overlap DMRs. To test whether variability in gene length might have contributed to the patterns we report, we took only DMGs with DMRs in their promoter region (-5 kb to +1 kb around the TSS). We observe very similar levels of enrichment (2.02x, 1.67x, and 1.24x, for vocal cords, larynx, and face, respectively, albeit FDR values > 0.05 due to low statistical power), suggesting that gene length does not affect the observed enrichment in genes affecting the face and larynx.

Additionally, to test whether cellular composition or differentiation state could bias the results, we ran Gene ORGANizer on the list of DMGs, following the removal of 20 DMRs that are found <10 kb from loci where methylation was shown to change during osteogenic differentiation (Håkelien et al., 2014). We found that genes affecting the voice and face are still the most over-represented (2.13x, 1.71x, and 1.27x, FDR = 0.032, FDR = 0.049, and FDR = 0.040, for vocal cords, larynx, and face, respectively, Table S4).

We also investigated the possibility that (for an unknown reason) the DMR-detection algorithm introduces positional biases that preferentially identify DMRs within genes affecting the voice or face. To this end, we simulated stochastic deamination processes along the Ust'-Ishim, Altai Neanderthal, and Denisovan genomes, reconstructed methylation maps, and ran the DMR-detection algorithm on these maps. We repeated this process 100 times for each hominin and found no enrichment of any body part, including the face, vocal cords, or larynx (1.07x, 1.07x, and 1.04x, respectively, FDR = 0.88 for vocal cords, larynx, and face). Perhaps most importantly, none of the other archaic branches shows enrichment of the larynx or the vocal cords. However, archaic-derived DMGs show over-representation of the jaws, as well as the lips, limbs, scapulae, and spinal column (Figure S1B, Table S4). In addition, DMRs that separate chimpanzees from all humans (archaic and modern, Table S2) do not show over-representation of genes that affect the voice, larynx, or face, compatible with the notion that this trend emerged along the MH lineage. Lastly, we added a human bone reduced representation bisulfite sequencing (RRBS) map (Wang et al., 2012), and produced a RRBS map from a chimpanzee infant unspecified long bone (Table S1, see Methods). RRBS methylation maps include information on only ~10% of CpG sites, and are biased towards unmethylated sites. Therefore, they were not included in the previous analyses. However, we added them in this part as they originate from a chimpanzee infant and a present-day human that is of similar age to the Denisovan (Table S1), allowing sampling from individuals that are younger than the rest. Repeating the Gene ORGANizer analysis after including these samples in the filtering process, we found that the face and larynx are the only significantly enriched skeletal regions, and the enrichment within voice-affecting genes becomes even more pronounced (2.33x, FDR = 7.9×10^{-3}, Table S4). Overall, we observe that MH-derived DMGs across all 60 MH samples are found outside archaic human variability, regardless of bone type, disease state, age, or

sex, and that chimpanzee methylation levels in these DMGs cluster closer to archaic humans than to MHs, suggesting that these factors are unlikely to underlie the observed trends.

Taken together, we conclude that DMGs that emerged along the MH lineage are uniquely enriched in genes affecting the voice and face, and that this is unlikely to be an artifact of (a) inter-individual variability resulting from age, sex, disease, or bone type; (b) significance level of DMRs; (c) the reconstruction or DMR-detection processes; (d) pleiotoropic effects of the genes; (e) the types of maps used in these processes; (f) the comparison of bone methylomes; or (g) gene length distribution.

Overall, we report 32 voice- and larynx-affecting DMGs. Disease-causing mutations in these genes have been shown to underlie various phenotypes, ranging from slight changes to the pitch and hoarseness of the voice, to a complete loss of speech ability (Table 1) (Gokhman et al., 2017a). These phenotypes were shown to be driven primarily by alterations to the laryngeal skeleton and vocal tract. Importantly, the laryngeal skeleton, and particularly the cricoid and arytenoid cartilages to which the vocal cords are anchored, are closest developmentally to limb bones, as these are the skeletal tissues that derive from the somatic layer of the lateral plate mesoderm. Methylation patterns in differentiated cells are often established during earlier stages of development, and the closer two tissues are developmentally, the higher the similarity between their methylation maps (Hernando-Herraez et al., 2015a, 2015b; Hon et al., 2013; Schultz et al., 2015; Ziller et al., 2013). Indeed, DMRs identified between species in one tissue often exist in other tissues as well (Hernando-Herraez et al., 2015b). Thus, it is likely that many of the DMRs identified here between limb samples also exist between laryngeal tissues. This is further supported by the observation that the methylation patterns in these DMGs appear in all examined skeletal samples, including femur, skull, rib, tibia, and tooth.

Extensive methylation changes within face and voice-affecting genes

Our results suggest that methylation levels in many face- and voice-affecting genes have changed since the split from archaic humans, but they do not provide information on the extent of changes within each gene. To do so, we scanned the genome in windows of 100 kb and computed the fraction of CpGs which are differentially methylated in MHs (hereinafter, MH-derived CpGs). We found that the extent of changes within voice-affecting DMGs is most profound, more than 2-fold compared to other DMGs (0.132 vs. 0.055, FDR = 2.3×10^{-3}, *t*-test, Table S5). Face-affecting DMGs also present high density of MH-derived CpGs (0.079 vs. 0.055, FDR = 2.8×10^{-3}). In archaic-derived DMGs, on the other hand, the extent of changes within voice- and face-affecting genes is not different than expected (FDR = 0.99, Table S5). To control for possible biases, we repeated the analysis using only the subset of DMRs in genes affecting the skeleton. Here too, we found that voice-affecting MH-derived DMGs present the highest density of changes (+154% for vocal cords, +140% for larynx, *FDR* = 1.4×10^{-3}, Table S5), and face-affecting DMGs also exhibit significantly elevated density of changes (+42% for face, FDR = 0.04).

Interestingly, when ranking DMGs according to the fraction of MH-derived CpGs, three of the top five, and all top five skeleton-related DMGs (*ACAN*, *SOX9*, *COL2A1*, *XYLT1*, and *NFIX*) affect lower and midfacial protrusion, as well as the voice (Frenzel et al., 1998; Lee and Saint-Jeannet, 2011; Meyer et al., 1997; Tompson et al., 2009) (Figure 4A,B). This is particularly surprising considering that genome-wide, less than 2% of genes (345) are known to affect the voice, ~3% of genes (726) are known to affect lower and midfacial protrusion, and less than 1% (182) are known to affect both. We also found that DMRs in voice- and face-affecting genes tend to be located ~20x closer than expected to MH-specific candidate positively selected loci (Peyrégne et al., 2017) ($P < 10^{-5}$, permutation test), and 50% closer compared to other MH-derived DMRs ($P < 10^{-5}$, Figure

282 4C). This is consistent with the possibility that some of these observations could have been driven
283 by positive selection.

284 The extra-cellular matrix genes *ACAN* and *COL2A1*, and their key regulator *SOX9*, form a network
285 of genes that regulate skeletal growth, the transition from cartilage to bone, and spatio-temporal
286 patterning of skeletal development, including facial and laryngeal skeleton in human (Lee and
287 Saint-Jeannet, 2011; Meyer et al., 1997) and mouse (Ng et al., 1997). *SOX9* is regulated by a
288 series of upstream enhancers identified in mouse and human (Bagheri-Fam et al., 2006; Sekido
289 and Lovell-Badge, 2008; Yao et al., 2015). In human skeletal samples, hypermethylation of the
290 *SOX9* promoter was shown to down-regulate its activity, and consequently its targets (Kim et al.,
291 2013). This was also demonstrated repeatedly in non-skeletal human (Aleman et al., 2008; Cheng
292 et al., 2015; Wagner et al., 2014) and mouse tissues (Huang et al., 2017; Pamnani et al., 2016). We
293 found substantial hypermethylation in MHs in the following regions: (a) the *SOX9* promoter; (b)
294 three of its proximal enhancers, including one that is active in mesenchymal cells (Yao et al.,
295 2015); (c) four of its skeletal enhancers; (d) the targets of SOX9 – *ACAN* (DMR #80) and *COL2A1*
296 (DMR #1, the most significant MH-derived DMR); and (e) an upstream lincRNA (*LINC02097*).
297 Notably, regions (a), (b), (c), and (e) are covered by the longest DMR on the MH-derived DMR
298 list, spanning 35,910 bp (DMR #11, Figure 5). Additionally, a more distant putative enhancer,
299 located 345kb upstream of *SOX9*, was shown to bear strong active histone modification marks in
300 chimpanzee craniofacial progenitor cells, whereas in humans these marks are almost absent (~10x
301 stronger in chimpanzee, suggesting down-regulation, Figure 5B) (Prescott et al., 2015).
302 Importantly, human and chimpanzee non-skeletal tissues (i.e., brain and blood) exhibit very similar
303 methylation patterns in these genes, suggesting they are bone-specific. Also, the amino acid
304 sequence coded by each of these genes is identical across the hominin groups (Prüfer et al., 2014),

suggesting that the changes along the MH lineage are purely regulatory. Together, these observations put forward the notion that *SOX9* became down-regulated in MH skeletal tissues, likely followed by down-regulation of its targets, *ACAN* and *COL2A1*.

XYLT1, the 4th highest skeleton-related DMG, is an enzyme involved in the synthesis of glycosaminoglycan. Loss-of-function mutations and reduced expression of the gene were shown to underlie the Desbuquois dysplasia skeletal syndrome, which was observed to affect the cartilaginous structure of the larynx, and drive a retraction of the face (Hall, 2001). Very little is known about *XYLT1* regulation, but interestingly, in zebrafish it was shown to be bound by SOX9 (Ohba et al., 2015).

NFIX methylation is inversely correlated with its expression

To further explore expression changes that are associated with changes in methylation, we scanned the DMRs to identify those whose methylation levels are strongly correlated with expression across 21 human tissues. We found 59 such MH-derived DMRs (FDR < 0.05). DMRs in voice-affecting genes are significantly more likely to be associated with expression compared to other DMRs (x2.05, $P = 6.65 \times 10^{-4}$, hypergeometric test). Particularly noteworthy is *NFIX*, one of the most derived genes in MHs (ranked 5th among DMGs affecting the skeleton, Figure 4A,B). *NFIX* has two DMRs (#24 and #167), and in both, methylation levels are tightly linked with expression, explaining 81.7% and 73.9% of its expression variation, respectively (FDR = 6.2×10^{-3} and 7.5×10^{-4}, Figure 6A-C). In fact, *NFIX* is one of the top ten DMGs with the most significant correlation between methylation and expression in human. The association between *NFIX* methylation and expression was also shown previously across several mouse tissues (Carrió et al., 2015; Maunakea et al., 2010), and suggests that the observed hypermethylation reflects down-regulation that

emerged along the MH lineage. Indeed, we found that *NFIX*, as well as *SOX9*, *ACAN*, *COL2A1*, and *XYLT1* show significantly reduced expression levels in humans compared to mice (Figure 6D). Most of the disease phenotypes that result from *NFIX* dysfunction are in the craniofacial region, as *NFIX* influences the balance between lower and upper projection of the face (Malan et al., 2010). In addition, mutations in *NFIX* were shown to impair speech capabilities (Shaw et al., 2010). Taken together, these observations suggest that DNA methylation is a primary mechanism in the regulation of *NFIX*, and serves as a good proxy for its expression. Interestingly, NFI proteins were shown to bind the upstream enhancers of *SOX9* (Pjanic et al., 2013), hence suggesting a possible mechanism to the simultaneous changes in these genes.

Discussion

Humans are distinguished from other apes in their unique capability to communicate through speech. This capacity is attributed not only to neural changes, but also to structural alterations to the vocal tract. The relative roles of anatomy and cognition in our speech skills are still debated, but it is nevertheless widely accepted that even with a human brain, other apes could not reach the human level of articulation (Fitch, 2000; Fitch et al., 2017; Lieberman, 2007, 2017). Nonhuman apes are restricted not only in their linguistic capacity (e.g., they can hardly learn grammar (Fitch, 2000)), but also in their ability to produce the phonetic range that humans can. Indeed, chimpanzees and bonobos communicate through sign language and symbols much better than they do vocally, even after being raised in an entirely human environment (Fitch, 2000). Phonetic range is determined by the different conformations that the vocal tract can produce. These conformations are largely shaped by the relative position of the larynx, tongue, lips, and mandible. Modern humans have a 1:1 proportion between the horizontal and vertical dimensions of the vocal tract,

which is unique among primates (Figure 6E) (Lieberman, 2007; Lieberman et al., 2001). It is still debated whether this configuration is a prerequisite for speech, but it was nonetheless shown to be optimal for speech (De Boer, 2010; Fitch, 2000; Lieberman, 2007; Lieberman et al., 2001). The 1:1 proportion was reached through retraction of the human face, together with the descent of the larynx (Lieberman, 2011).

A longstanding question is whether Neanderthals and modern humans share similar vocal anatomy (Boë et al., 2002; Fitch, 2000; Lieberman P. and McCarthy C., 2014; Steele et al., 2013). Attempts to answer this question based on morphological differences between the two human groups have proven hard, as the larynx is mostly composed of soft tissues (e.g., cartilage), which do not survive long after death. The only remnant from the Neanderthal laryngeal region is the hyoid bone (Fitch, 2000; Steele et al., 2013). Based on this single bone, or on computer simulations and tentative vocal tract reconstructions, it is difficult to characterize the full anatomy of the Neanderthal vocal apparatus, and opinions remain split as to whether it was similar to modern humans (Boë et al., 2002; Fitch, 2000; Lieberman P. and McCarthy C., 2014; Steele et al., 2013).

The results we report, which are based on reconstructions of ancient DNA methylation patterns, provide a novel means to analyze the mechanisms that underlie the evolution of the human face and vocal tract. We have shown here that genes affecting vocal and facial anatomy went through extensive methylation changes in recent MH evolution, following the split from Neanderthals and Denisovans. These alterations are manifested both in the number of divergent genes and in the extent of changes within each gene. The DMRs we report capture substantial methylation changes (over 50% between at least one pair of human groups), span thousands or tens of thousands of bases, and cover regulatory regions such as promoters and enhancers. Many of these methylation changes were shown here and in previous works to be tightly linked with changes in expression

levels. We particularly focused on changes in the regulation of the five most diverged genes on the MH lineage: *SOX9*, *ACAN*, *COL2A1*, *XYLT1*, and *NFIX*, which are all associated with a range of skeletal phenotypes, and whose downregulation was shown to underlie a retracted face, as well as changes to the structure of the larynx.

In this paper, we argue for possible interplay between methylation changes and phenotypic effects. Such links are not straightforward, because almost all studies linking genes to diseases and phenotypes seek sequence mutations, and particularly those that affect protein sequence. Nevertheless, many diseases-causing genetic variants are loss-of-function mutations, especially those that cause haploinsufficiency, and their effect could be roughly paralleled to partial silencing of a gene. Therefore, phenotypes associated with such loss-of-function genetic variants could be regarded as consequences of reduced gene activity in humans. To support our inference on the facial and laryngeal phenotypic impacts of methylation changes in *SOX9*, *ACAN*, *COL2A1*, *XYLT1*, and *NFIX* we verified that these phenotypes are indeed a result of loss-of-function mutations.

NFIX poses a particularly interesting example, as the methylation levels in its two DMRs strongly predict its expression level (Figure 6B,C). To investigate whether changes in *NFIX* expression could explain some specific morphological changes in MH face and larynx, we examined its skeletal phenotypes. Mutations in *NFIX* were shown to be behind the Marshall-Smith and Malan syndromes, whose phenotypes include various skeletal alterations such as hypoplasia of the midface, retracted lower jaw, and depressed nasal bridge (Malan et al., 2010), as well as limited speech capabilities (Shaw et al., 2010). In many of the patients, the phenotypic alterations are driven by heterozygous loss-of-function mutations causing haploinsufficiency, showing that changes in NFIX dosage affect skeletal morphology (Malan et al., 2010). Given that reduced

activity of *NFIX* drives these symptoms, a possible hypothesis is that increased *NFIX* activity in the Neanderthal would result in phenotypic changes in the opposite direction. Such opposite phenotypic effects of under- and over-expression of genes has been demonstrated previously in hundreds of genes, and especially within transcription factors (Dang et al., 2008; Hamosh et al., 2005; Strande et al., 2017). Indeed, we found this to be the case in 18 out of 22 Marshall-Smith syndrome skeletal phenotypes, and in 8 out of 9 Malan syndrome skeletal phenotypes. In other words, from the syndromes driven by *NFIX* haploinsufficiency, through healthy MHs, to the Neanderthal, the level of phenotype manifestation corresponds to the level of *NFIX* activity (Figure 6F, Table S6). Interestingly, many cases of laryngeal malformations in the Marshall-Smith syndrome have been reported (Cullen et al., 1997). Some of the patients exhibit positional changes of the larynx, changes in its width, and structural alterations to the arytenoid cartilage – the anchor point of the vocal cords, which controls their movement (Cullen et al., 1997). In fact, these laryngeal and facial anatomical changes are thought to underlie the limited speech capabilities observed in some patients (Shaw et al., 2010).

In light of the role of facial flattening in determining speech capabilities, it is illuminating that flattening of the face is the most common phenotype associated with reduced activity of *SOX9*, *ACAN*, and *COL2A1* (Gokhman et al., 2017a). Heterozygous loss-of-function mutations in *SOX9*, which result in a reduction of ~50% in its activity, were shown to cause a retracted lower face, and to affect the pitch of the voice (Lee and Saint-Jeannet, 2011; Meyer et al., 1997). *ACAN* was shown to affect facial prognathism and the hoarseness of the voice (Tompson et al., 2009). *COL2A1* is key for proper laryngeal skeletal development (Frenzel et al., 1998), and its decreased activity results in a retracted face (Hoornaert et al., 2010). The lower and midface of MHs is markedly retracted not only compared to apes, but also to Australopithecines and other *Homo* groups,

418 including the Neanderthal (Lieberman, 2011). The developmental alterations that underlie the
419 ontogeny of the human face, however, are still under investigation. Cranial base length and flexion
420 were shown to play a role in the retracted face, as well as in vocal tract length (Aiello and Dean,
421 2002; Lieberman, 1998, 2011), but reduced growth rate and heterochrony of spatio-temporal
422 switches are thought to be involved as well (Bastir et al., 2007). Importantly, *SOX9* and *COL2A1*
423 were implicated in the elongation and ossification of the cranial base (Horton WA, Rimoin DL,
424 Hollister DW, 1979; Yan et al., 2005), and the methylation patterns we report all exist in the cranial
425 base sample (I1583). Additionally, *SOX9* is a key regulator of skeletal growth rate, and the
426 developmental switch to ossification (Lee and Saint-Jeannet, 2011; Meyer et al., 1997).
427 Importantly, facial retraction also occurred before the split of archaic and modern humans, and the
428 faces of hominins are substantially shorter than those of chimpanzees and bonobos (Lieberman,
429 2011). Therefore, the DMGs we report could potentially be associated with recent facial retraction
430 in MHs, but not with morphological changes that precede the split.

431 We identified DMRs in *SOX9*, *ACAN*, *COL2A1*, *XYLT1*, and *NFIX* as some of the most derived
432 loci in MHs. These genes are active mainly in early stages of osteochondrogenesis, making the
433 observation of differential methylation in mature bones puzzling at first glance. This could
434 potentially be explained by two factors: (i) The DMRs might reflect early methylation changes in
435 the mesenchymal progenitors of these cells that are carried on to later stages of osteogenesis. This
436 possibility is supported by previous observations of many regulatory regions that are active during
437 early development and maintain their active methylation marks in adult tissues, despite becoming
438 inactive. In such regions, adult methylation states reflect earlier development, and DMRs in adult
439 stages could reflect heterochrony or earlier alterations in activity levels (Hernando-Herraez et al.,
440 2015a; Hon et al., 2013; Schultz et al., 2015). It is also supported by the observation that the

methylation patterns of *NFIX*, *SOX9*, *ACAN*, and *COL2A1* are established in early stages of development and remain stable throughout differentiation from mesenchymal stem cells to osteocytes (Håkelien et al., 2014). Additionally, we show that the upstream mesenchymal enhancer of *SOX9* (Yao et al., 2015) is differentially methylated in MHs (Figure 5B). (ii) Although expression levels of *SOX9*, *ACAN*, and *COL2A1* gradually decrease with the progress towards skeletal maturation, these genes were shown to be still expressed in later skeletal developmental stages in the larynx, vertebrae, limbs, and jaws, including in their osteoblasts (Moriarity et al., 2015; Ng et al., 1997; Rojas-Peña et al., 2014). Interestingly, these are also the organs that are most affected by mutations in these genes, implying that late stages of activity of these genes might still play important roles in morphological patterning (Frenzel et al., 1998; Hoornaert et al., 2010; Lee and Saint-Jeannet, 2011; Meyer et al., 1997; Tompson et al., 2009). It was also shown that facial growth patterns, which shape facial prognathism, differ between archaic and modern humans not only during early development, but also as late as adolescence (Lacruz et al., 2015).

To further investigate potential phenotypic consequences of the DMGs we report, we probed the HPO database (Köhler et al., 2014). For each skeletal-affecting phenotype, we determined whether it matches a known morphological difference between Neanderthals and MHs. For example, *FGFR3* was shown to affect the size of the iliac bones (HPO ID: HP:0000946), and in the Neanderthal, these bones are considerably hyperplastic compared to MHs (Weaver, 2009). We then counted for each gene (whether DMG or not) the fraction of its associated HPO phenotypes that are divergent between Neanderthals and MHs. We found that four out of the top five most differentially methylated genes (*XYLT1*, *NFIX*, *ACAN*, and *COL2A1*) are found within the top 100 genes with the highest fraction of traits where Neanderthals and MHs differ (out of a total of 1,789 skeleton-related genes). In fact, *COL2A1*, which is the most differentially methylated gene, is also

464 the gene associated with the most derived traits (63) compared to all genes throughout the genome
465 (Table S7).

466 DNA methylation in some loci differs between cell types and sexes, changes with age, and might
467 be affected by factors such as environment and diet (Gokhman et al., 2017b). In this work, we took
468 measures to exclude such DMRs and to focus on DMRs that likely represent evolutionary
469 differences between the human groups. This was done by combining information from diverse
470 methylation maps. In MH-derived DMRs, for example, we use only DMRs in which chimpanzees
471 and archaic humans form a cluster that is distinct from the cluster of MHs (Figure 2A). Each of
472 the two clusters contains samples from females and males, and from a variety of ages and bones
473 (Table S1). Additionally, we show that these DMRs hold even when comparing methylation maps
474 produced using the same technology, and from the same bone type, sex, and age group (Figure
475 S2A,B). Therefore, the observed differences are unlikely to be driven by these factors, but rather
476 add credence to the notion that they reflect MH-specific evolutionary shifts. This is further
477 supported by the phenotypic observations that facial prognathism in general, and facial growth
478 rates in particular, are derived and reduced in MHs (Lacruz et al., 2015).

479 The results we presented here open a window to study the evolution of the MH face and vocal tract
480 from a genetic perspective. Our data suggest shared genetic mechanisms that shaped these
481 anatomical regions and point to evolutionary events that separate MHs from the Neanderthal and
482 Denisovan. The mechanisms leading to such extensive regulatory shifts, as well as if and to what
483 extent these evolutionary changes affected speech capabilities are still to be determined.

References

Aiello, L., and Dean, C. (2002). An Introduction to Human Evolutionary Anatomy (London: Elsevier).

Aleman, A., Adrien, L., Lopez-Serra, L., Cordon-Cardo, C., Esteller, M., Belbin, T.J., and Sanchez-Carbayo, M. (2008). Identification of DNA hypermethylation of SOX9 in association with bladder cancer progression using CpG microarrays. Br. J. Cancer *98*, 466–473.

Altschul, S.F., Madden, T.L., Schäffer, A.A., Zhang, J., Zhang, Z., Miller, W., and Lipman, D.J. (1997). Gapped BLAST and PSI-BLAST: a new generation of protein database search programs. Nucleic Acids Res. *25*, 3389–3402.

Aryee, M.J., Jaffe, A.E., Corrada-Bravo, H., Ladd-Acosta, C., Feinberg, A.P., Hansen, K.D., and Irizarry, R.A. (2014). Minfi: a flexible and comprehensive Bioconductor package for the analysis of Infinium DNA methylation microarrays. Bioinformatics *30*, 1363–1369.

Ayturk, U.M., Jacobsen, C.M., Christodoulou, D.C., Gorham, J., Seidman, J.G., Seidman, C.E., Robling, A.G., and Warman, M.L. (2013). An RNA-seq protocol to identify mRNA expression changes in mouse diaphyseal bone: Applications in mice with bone property altering Lrp5 mutations. J. Bone Miner. Res. *28*, 2081–2093.

Bagheri-Fam, S., Barrionuevo, F., Dohrmann, U., Günther, T., Schüle, R., Kemler, R., Mallo, M., Kanzler, B., and Scherer, G. (2006). Long-range upstream and downstream enhancers control distinct subsets of the complex spatiotemporal Sox9 expression pattern. Dev. Biol. *291*, 382–397.

Barnett, R., and Larson, G. (2012). A phenol-chloroform protocol for extracting DNA from ancient samples. Methods Mol. Biol. *840*, 13–19.

Bastir, M., O'Higgins, P., and Rosas, A. (2007). Facial ontogeny in Neanderthals and modern humans. Proc. R. Soc. B Biol. Sci. *274*, 1125–1132.

506 Been, E., Gõmez-Olivencia, A., and Kramer, P.A. (2012). Lumbar lordosis of extinct hominins. Am. J.
507 Phys. Anthropol. *147*, 64–77.

508 Boë, L.-J., Heim, J.-L., Honda, K., and Maeda, S. (2002). The potential Neandertal vowel space was as
509 large as that of modern humans. J. Phon. *30*, 465–484.

510 De Boer, B. (2010). Modelling vocal anatomy's significant effect on speech. J. Evol. Psychol. *8*, 351–366.

511 Boyle, P., Clement, K., Gu, H., Smith, Z.D., Ziller, M., Fostel, J.L., Holmes, L., Meldrim, J., Kelley, F.,
512 Gnirke, A., et al. (2012). Gel-free multiplexed reduced representation bisulfite sequencing for large-scale
513 DNA methylation profiling. Genome Biol. *13*, R92.

514 Briggs, A.W., Stenzel, U., Meyer, M., Krause, J., Kircher, M., and Pääbo, S. (2010). Removal of
515 deaminated cytosines and detection of in vivo methylation in ancient DNA. Nucleic Acids Res. *38*, e87.

516 Carrió, E., Díez-Villanueva, A., Lois, S., Mallona, I., Cases, I., Forn, M., Peinado, M.A., and Suelves, M.
517 (2015). Deconstruction of DNA methylation patterns during myogenesis reveals specific epigenetic events
518 in the establishment of the skeletal muscle lineage. Stem Cells *33*, 2025–2036.

519 Cheng, P.F., Shakhova, O., Widmer, D.S., Eichhoff, O.M., Zingg, D., Frommel, S.C., Belloni, B.,
520 Raaijmakers, M.I., Goldinger, S.M., Santoro, R., et al. (2015). Methylation-dependent SOX9 expression
521 mediates invasion in human melanoma cells and is a negative prognostic factor in advanced melanoma.
522 Genome Biol. *16*, 42.

523 Clement, A.F., Hillson, S.W., and Aiello, L.C. (2012). Tooth wear, Neanderthal facial morphology and the
524 anterior dental loading hypothesis. J. Hum. Evol. *62*, 367–376.

525 Cullen, A., Clarke, T.A., and O'Dwyer, T.P. (1997). The Marshall-Smith syndrome: a review of the
526 laryngeal complications. Eur J Pediatr *156*, 463–464.

527 Dabney, J., Knapp, M., Glocke, I., Gansauge, M.-T., Weihmann, A., Nickel, B., Valdiosera, C., García, N.,

528 Pääbo, S., Arsuaga, J.-L., et al. (2013). Complete mitochondrial genome sequence of a Middle Pleistocene
529 cave bear reconstructed from ultrashort DNA fragments. Proc. Natl. Acad. Sci. U. S. A. *110*, 15758–15763.

530 Dang, V.T., Kassahn, K.S., Marcos, A.E., and Ragan, M.A. (2008). Identification of human
531 haploinsufficient genes and their genomic proximity to segmental duplications. Eur. J. Hum. Genet. *16111*,
532 1350–1357.

533 Fitch, W.T. (2000). The evolution of speech: A comparative review. Trends Cogn. Sci. *4*, 258–267.

534 Fitch, W.T., de Boer, B., Mathur, N., and A. Ghazanfar, A. (2017). Response to Lieberman on "Monkey
535 vocal tracts are speech-ready." Sci. Adv. *3*.

536 Fortin, J.-P., Labbe, A., Lemire, M., Zanke, B.W., Hudson, T.J., Fertig, E.J., Greenwood, C.M., and
537 Hansen, K.D. (2014). Functional normalization of 450k methylation array data improves replication in large
538 cancer studies. Genome Biol. *15*, 503.

539 Fortin, J.-P., Triche, T., and Hansen, K. (2016). Preprocessing, normalization and integration of the Illumina
540 HumanMethylationEPIC array. bioRxiv 65490.

541 Fraser, H.B. (2013). Gene expression drives local adaptation in humans. Genome Res. *23*, 1089–1096.

542 Frenzel, K., Amann, G., and Lubec, B. (1998). Deficiency of laryngeal collagen type II in an infant with
543 respiratory problems. Arch. Dis. Child. *78*, 557–559.

544 Fu, Q., Li, H., Moorjani, P., Jay, F., Slepchenko, S.M., Bondarev, A.A., Johnson, P.L.F., Aximu-Petri, A.,
545 Prüfer, K., de Filippo, C., et al. (2014). Genome sequence of a 45,000-year-old modern human from western
546 Siberia. Nature *514*, 445–449.

547 Gokhman, D., Lavi, E., Prüfer, K., Fraga, M.F., Riancho, J.A., Kelso, J., Pääbo, S., Meshorer, E., and
548 Carmel, L. (2014). Reconstructing the DNA methylation maps of the Neandertal and the Denisovan.
549 Science *344*, 523–527.

550 Gokhman, D., Meshorer, E., and Carmel, L. (2016). Epigenetics: It's Getting Old. Past Meets Future in
551 Paleoepigenetics. Trends Ecol. Evol. *31*.

552 Gokhman, D., Kelman, G., Amartely, A., Gershon, G., Tsur, S., and Carmel, L. (2017a). Gene ORGANizer:
553 Linking genes to the organs they affect. Nucleic Acids Res. *45*.

554 Gokhman, D., Malul, A., and Carmel, L. (2017b). Inferring Past Environments from Ancient Epigenomes.
555 Mol. Biol. Evol. *msx211*.

556 Gómez-Olivencia, A., Been, E., Arsuaga, J.L., and Stock, J.T. (2013). The Neandertal vertebral column 1:
557 The cervical spine. J. Hum. Evol. *64*, 608–630.

558 De Groote, I. (2011). The Neanderthal lower arm. J. Hum. Evol. *61*, 396–410.

559 De Groote, I.E.P.M. (2008). A comprehensive analysis of long bone curvature in Neanderthals and Modern
560 Humans using 3D morphometrics. University College London.

561 Haak, W., Lazaridis, I., Patterson, N., Rohland, N., Mallick, S., Llamas, B., Brandt, G., Nordenfelt, S.,
562 Harney, E., Stewardson, K., et al. (2015). Massive migration from the steppe was a source for Indo-
563 European languages in Europe. Nature *522*, 207–211.

564 Håkelien, A.M., Bryne, J.C., Harstad, K.G., Lorenz, S., Paulsen, J., Sun, J., Mikkelsen, T.S., Myklebost,
565 O., and Meza-Zepeda, L.A. (2014). The regulatory landscape of osteogenic differentiation. Stem Cells *32*,
566 2780–2793.

567 Hall, B.D. (2001). Lethality in Desbuquois dysplasia: Three new cases. Pediatr. Radiol. *31*, 43–47.

568 Hamosh, A., Scott, A.F., Amberger, J.S., Bocchini, C.A., and McKusick, V.A. (2005). Online Mendelian
569 Inheritance in Man (OMIM), a knowledgebase of human genes and genetic disorders. Nucleic Acids Res.
570 *33*.

571 Hanghøj, K., Seguin-Orlando, A., Schubert, M., Madsen, T., Pedersen, J.S., Willerslev, E., and Orlando, L.

(2016). Fast, Accurate and Automatic Ancient Nucleosome and Methylation Maps with epiPALEOMIX. Mol. Biol. Evol. *33*, 3284–3298.

Hernando-Herraez, I., Prado-Martinez, J., Garg, P., Fernandez-Callejo, M., Heyn, H., Hvilsom, C., Navarro, A., Esteller, M., Sharp, A.J., and Marques-Bonet, T. (2013). Dynamics of DNA Methylation in Recent Human and Great Ape Evolution. PLOS Genet *9*, e1003763.

Hernando-Herraez, I., Garcia-Perez, R., Sharp, A.J., and Marques-Bonet, T. (2015a). DNA Methylation: Insights into Human Evolution. PLoS Genet. *11*.

Hernando-Herraez, I., Heyn, H., Fernandez-Callejo, M., Vidal, E., Fernandez-Bellon, H., Prado-Martinez, J., Sharp, A.J., Esteller, M., and Marques-Bonet, T. (2015b). The interplay between DNA methylation and sequence divergence in recent human evolution. Nucleic Acids Res *43*, 8204–8214.

Hon, G.C., Rajagopal, N., Shen, Y., McCleary, D.F., Yue, F., Dang, M.D., and Ren, B. (2013). Epigenetic memory at embryonic enhancers identified in DNA methylation maps from adult mouse tissues. Nat. Genet. *45*, 1198–1206.

Hoornaert, K.P., Vereecke, I., Dewinter, C., Rosenberg, T., Beemer, F.A., Leroy, J.G., Bendix, L., Björck, E., Bonduelle, M., Boute, O., et al. (2010). Stickler syndrome caused by COL2A1 mutations: genotype–phenotype correlation in a series of 100 patients. Eur J Hum Genet. *18*, 872–880.

Horton WA, Rimoin DL, Hollister DW, L.R. (1979). Further heterogeneity within lethal neonatal short-limbed dwarfism: the platyspondylic types. J Pediatr. *94*, 736–742.

Horvath, S., Mah, V., Lu, A.T., Woo, J.S., Choi, O.W., Jasinska, A.J., Riancho, J.A., Tung, S., Coles, N.S., Braun, J., et al. (2015). The cerebellum ages slowly according to the epigenetic clock. Aging (Albany. NY). *7*, 294–306.

Huang, C.-Z., Xu, J.-H., Zhong, W., Xia, Z.-S., Wang, S.-Y., Cheng, D., Li, J.-Y., Wu, T.-F., Chen, Q.-K.,

and Yu, T. (2017). Sox9 transcriptionally regulates Wnt signaling in intestinal epithelial stem cells in hypomethylated crypts in the diabetic state. Stem Cell Res. Ther. *8*, 60.

Huang, D.W., Lempicki, R. a, and Sherman, B.T. (2009). Systematic and integrative analysis of large gene lists using DAVID bioinformatics resources. Nat. Protoc. *4*, 44–57.

Huber, W., Carey, V.J., Gentleman, R., Anders, S., Carlson, M., Carvalho, B.S., Bravo, H.C., Davis, S., Gatto, L., Girke, T., et al. (2015). Orchestrating high-throughput genomic analysis with Bioconductor. Nat. Methods *12*, 115–121.

Kanehisa, M., Sato, Y., Kawashima, M., Furumichi, M., and Tanabe, M. (2016). KEGG as a reference resource for gene and protein annotation. Nucleic Acids Res. *44*, D457–D462.

Kim, K. Il, Park, Y.S., and Im, G. Il (2013). Changes in the epigenetic status of the SOX-9 promoter in human osteoarthritic cartilage. J. Bone Miner. Res. *28*, 1050–1060.

King, M.C., and Wilson, A.C. (1975). Evolution at two levels in humans and chimpanzees. Science *188*, 107–116.

Köhler, S., Doelken, S.C., Mungall, C.J., Bauer, S., Firth, H. V., Bailleul-Forestier, I., Black, G.C.M., Brown, D.L., Brudno, M., Campbell, J., et al. (2014). The Human Phenotype Ontology project: Linking molecular biology and disease through phenotype data. Nucleic Acids Res. *42*.

Kupczik, K., and Hublin, J.J. (2010). Mandibular molar root morphology in Neanderthals and Late Pleistocene and recent Homo sapiens. J. Hum. Evol. *59*, 525–541.

Lacruz, R.S., Bromage, T.G., O'Higgins, P., Arsuaga, J.-L., Stringer, C., Godinho, R.M., Warshaw, J., Martínez, I., Gracia-Tellez, A., de Castro, J.M.B., et al. (2015). Ontogeny of the maxilla in Neanderthals and their ancestors. Nat. Commun. *6*, 8996.

Lazaridis, I., Patterson, N., Mittnik, A., Renaud, G., Mallick, S., Sudmant, P.H., Schraiber, J.G., Castellano,

S., Kirsanow, K., Economou, C., et al. (2014). Ancient human genomes suggest three ancestral populations for present-day Europeans. Nature *513*, 409–413.

Lee, Y.H., and Saint-Jeannet, J.P. (2011). Sox9 function in craniofacial development and disease. Genesis *49*, 200–208.

Lieberman, D.E. (1998). Sphenoid shortening and the evolution of modern human cranial shape. Nature *393*, 158–162.

Lieberman, D.E. (2011). The Evolution of the Human Head (Harvard University Press).

Lieberman, P. (2007). The Evolution of Human Speech: Its Anatomical and Neural Bases. Curr. Anthropol. *48*, 39–66.

Lieberman, P. (2017). Comment on "Monkey vocal tracts are speech-ready." Sci. Adv. *3*.

Lieberman, D.E., Pearson, O.M., and Mowbray, K.M. (2000). Basicranial influence on overall cranial shape. J. Hum. Evol. *38*, 291–315.

Lieberman, D.E., McCarthy, R.C., Hiiemae, K.M., and Palmer, J.B. (2001). Ontogeny of postnatal hyoid and larynx descent in humans. Arch. Oral Biol. *46*, 117–128.

Lieberman P. and McCarthy C. (2014). The Evolution of Speech and Language. Handb. Paleoanthropology.

Lokk, K., Modhukur, V., Rajashekar, B., Märtens, K., Mägi, R., Kolde, R., Koltšina, M., Nilsson, T.K., Vilo, J., Salumets, A., et al. (2014). DNA methylome profiling of human tissues identifies global and tissue-specific methylation patterns. Genome Biol. *15*, r54.

Malan, V., Rajan, D., Thomas, S., Shaw, A.C., Louis Dit Picard, H., Layet, V., Till, M., Van Haeringen, A., Mortier, G., Nampoothiri, S., et al. (2010). Distinct effects of allelic NFIX mutations on nonsense-mediated mRNA decay engender either a sotos-like or a Marshall-Smith Syndrome. Am. J. Hum. Genet. *87*, 189–198.

638 Martynoga, B., Mateo, J.L., Zhou, B., Andersen, J., Achimastou, A., Urbán, N., van den Berg, D.,
639 Georgopoulou, D., Hadjur, S., Wittbrodt, J., et al. (2013). Epigenomic enhancer annotation reveals a key
640 role for NFIX in neural stem cell quiescence. Genes Dev. *27*, 1769–1786.

641 Mathieson, I., Lazaridis, I., Rohland, N., Mallick, S., Patterson, N., Roodenberg, S.A., Harney, E.,
642 Stewardson, K., Fernandes, D., Novak, M., et al. (2015). Genome-wide patterns of selection in 230 ancient
643 Eurasians. Nature *528*, 499–503.

644 Maunakea, A.K., Nagarajan, R.P., Bilenky, M., Ballinger, T.J., D'Souza, C., Fouse, S.D., Johnson, B.E.,
645 Hong, C., Nielsen, C., Zhao, Y., et al. (2010). Conserved role of intragenic DNA methylation in regulating
646 alternative promoters. Nature *466*, 253–257.

647 Maureille, B., and Bar, D. (1999). The premaxilla in Neandertal and early modern children: ontogeny and
648 morphology. J. Hum. Evol. *37*, 137–152.

649 McCartney, D.L., Walker, R.M., Morris, S.W., McIntosh, A.M., Porteous, D.J., and Evans, K.L. (2016).
650 Identification of polymorphic and off-target probe binding sites on the Illumina Infinium MethylationEPIC
651 BeadChip. Genomics Data *9*, 22–24.

652 Meyer, J., Südbeck, P., Held, M., Wagner, T., Schmitz, M.L., Dagna Bricarelli, F., Eggermont, E.,
653 Friedrich, U., Haas, O.A., Kobelt, A., et al. (1997). Mutational analysis of the SOX9 gene in campomelic
654 dysplasia and autosomal sex reversal: Lack of genotype/phenotype correlations. Hum. Mol. Genet. *6*, 91–
655 98.

656 Meyer, M., Kircher, M., Gansauge, M.-T., Li, H., Racimo, F., Mallick, S., Schraiber, J.G., Jay, F., Prüfer,
657 K., de Filippo, C., et al. (2012). A high-coverage genome sequence from an archaic Denisovan individual.
658 Science *338*, 222–226.

659 Moriarity, B.S., Otto, G.M., Rahrmann, E.P., Rathe, S.K., Wolf, N.K., Weg, M.T., Manlove, L.A., LaRue,
660 R.S., Temiz, N.A., Molyneux, S.D., et al. (2015). A Sleeping Beauty forward genetic screen identifies new

661 genes and pathways driving osteosarcoma development and metastasis. Nat. Genet. *47*, 615–624.

662 Ng, L.J., Wheatley, S., Muscat, G.E., Conway-Campbell, J., Bowles, J., Wright, E., Bell, D.M., Tam, P.P.,
663 Cheah, K.S., and Koopman, P. (1997). Sox9 binds DNA, activates transcription, and coexpresses with type
664 II collagen during chondrogenesis in the mouse. Dev. Biol. *183*, 108–121.

665 Ohba, S., He, X., Hojo, H., and McMahon, A.P. (2015). Distinct Transcriptional Programs Underlie Sox9
666 Regulation of the Mammalian Chondrocyte. Cell Rep. *12*, 229–243.

667 Olalde, I., Allentoft, M.E., Sánchez-Quinto, F., Santpere, G., Chiang, C.W.K., DeGiorgio, M., Prado-
668 Martinez, J., Rodríguez, J.A., Rasmussen, S., Quilez, J., et al. (2014). Derived immune and ancestral
669 pigmentation alleles in a 7,000-year-old Mesolithic European. Nature *507*, 225–228.

670 Ong, M.-L., Tan, P.Y., MacIsaac, J.L., Mah, S.M., Buschdorf, J.P., Cheong, C.Y., Stunkel, W., Chan, L.,
671 Gluckman, P.D., Chng, K., et al. (2014). Infinium Monkeys: Infinium 450K Array for the Cynomolgus
672 macaque (Macaca fascicularis). G3 Genes|Genomes|Genetics *4*, 1227–1234.

673 Page, E. (1954). Continuous inspection schemes. Biometrika *41*, 100–115.

674 Pamnani, M., Sinha, P., Singh, A., Nara, S., and Sachan, M. (2016). Methylation of the Sox9 and Oct4
675 promoters and its correlation with gene expression during testicular development in the laboratory mouse.
676 Genet. Mol. Biol. *39*, 452–458.

677 Pedersen, J.S., Valen, E., Velazquez, A.M.V., Parker, B.J., Rasmussen, M., Lindgreen, S., Lilje, B., Tobin,
678 D.J., Kelly, T.K., Vang, S., et al. (2014). Genome-wide nucleosome map and cytosine methylation levels
679 of an ancient human genome. Genome Res. *24*, 454–466.

680 Peyrégne, S., Boyle, M.J., Dannemann, M., and Prüfer, K. (2017). Detecting ancient positive selection in
681 humans using extended lineage sorting. Genome Res. *27*, 1563–1572.

682 Pjanic, M., Schmid, C.D., Gaussin, A., Ambrosini, G., Adamcik, J., Pjanic, P., Plasari, G., Kerschgens, J.,

683 Dietler, G., Bucher, P., et al. (2013). Nuclear Factor I genomic binding associates with chromatin
684 boundaries. BMC Genomics *14*, 99.

685 Prescott, S.L., Srinivasan, R., Marchetto, M.C., Grishina, I., Narvaiza, I., Selleri, L., Gage, F.H., Swigut,
686 T., and Wysocka, J. (2015). Enhancer Divergence and cis-Regulatory Evolution in the Human and Chimp
687 Neural Crest. Cell *163*, 68–84.

688 Prideaux, M., Dallas, S.L., Zhao, N., Johnsrud, E.D., Veno, P.A., Guo, D., Mishina, Y., Harris, S.E., and
689 Bonewald, L.F. (2015). Parathyroid hormone induces bone cell motility and loss of mature osteocyte
690 phenotype through L-calcium channel dependent and independent mechanisms. PLoS One *10*.

691 Prüfer, K., Racimo, F., Patterson, N., Jay, F., Sankararaman, S., Sawyer, S., Heinze, A., Renaud, G.,
692 Sudmant, P.H., de Filippo, C., et al. (2014). The complete genome sequence of a Neanderthal from the Altai
693 Mountains. Nature *505*, 43–49.

694 Raichlen, D.A., Armstrong, H., and Lieberman, D.E. (2011). Calcaneus length determines running
695 economy: Implications for endurance running performance in modern humans and Neandertals. J. Hum.
696 Evol. *60*, 299–308.

697 Reich, D., Green, R.E., Kircher, M., Krause, J., Patterson, N., Durand, E.Y., Viola, B., Briggs, A.W.,
698 Stenzel, U., Johnson, P.L.F., et al. (2010). Genetic history of an archaic hominin group from Denisova Cave
699 in Siberia. Nature *468*, 1053–1060.

700 Roadmap Epigenomics Consortium, Kundaje, A., Meuleman, W., Ernst, J., Bilenky, M., Yen, A., Heravi-
701 Moussavi, A., Kheradpour, P., Zhang, Z., Wang, J., et al. (2015). Integrative analysis of 111 reference
702 human epigenomes. Nature *518*, 317–329.

703 Rohland, N., and Hofreiter, M. (2007). Ancient DNA extraction from bones and teeth. Nat. Protoc. *2*, 1756–
704 1762.

Rojas-Peña, M.L., Olivares-Navarrete, R., Hyzy, S., Arafat, D., Schwartz, Z., Boyan, B.D., Williams, J., and Gibson, G. (2014). Characterization of distinct classes of differential gene expression in osteoblast cultures from non-syndromic craniosynostosis bone. J. Genomics *2*, 121–130.

Schultz, M.D., He, Y., Whitaker, J.W., Hariharan, M., Mukamel, E.A., Leung, D., Rajagopal, N., Nery, J.R., Urich, M.A., Chen, H., et al. (2015). Human body epigenome maps reveal noncanonical DNA methylation variation. Nature *523*, 212–216.

Sekido, R., and Lovell-Badge, R. (2008). Sex determination involves synergistic action of SRY and SF1 on a specific Sox9 enhancer. Nature *453*, 930–934.

Shaw, A.C., Van Balkom, I.D.C., Bauer, M., Cole, T.R.P., Delrue, M.A., Van Haeringen, A., Holmberg, E., Knight, S.J.L., Mortier, G., Nampoothiri, S., et al. (2010). Phenotype and natural history in Marshall-Smith syndrome. Am. J. Med. Genet. Part A *152*, 2714–2726.

Siegmund, D.O., Zhang, N.R., and Yakir, B. (2011). False discovery rate for scanning statistics. Biometrika *98*, 979–985.

Simbolo, M., Gottardi, M., Corbo, V., Fassan, M., Mafficini, A., Malpeli, G., Lawlor, R.T., and Scarpa, A. (2013). DNA Qualification Workflow for Next Generation Sequencing of Histopathological Samples. PLoS One *8*.

Steele, J., Clegg, M., and Martelli, S. (2013). Comparative morphology of the hominin and african ape hyoid bone, a possible marker of the evolution of speech. Hum Biol *85*, 639–672.

Strande, N.T., Riggs, E.R., Buchanan, A.H., Ceyhan-Birsoy, O., DiStefano, M., Dwight, S.S., Goldstein, J., Ghosh, R., Seifert, B.A., Sneddon, T.P., et al. (2017). Evaluating the Clinical Validity of Gene-Disease Associations: An Evidence-Based Framework Developed by the Clinical Genome Resource. Am. J. Hum. Genet. *100*, 895–906.

727 Tharmaratnam, K., Sperrin, M., Jaki, T., Reppe, S., Frigessi, A., Tibshirani, R., Zhao, P., Yu, B., Zou, H.,
728 Bunea, F., et al. (2016). Tilting the lasso by knowledge-based post-processing. BMC Bioinformatics *17*,
729 344.

730 Tompson, S.W., Merriman, B., Funari, V.A., Fresquet, M., Lachman, R.S., Rimoin, D.L., Nelson, S.F.,
731 Briggs, M.D., Cohn, D.H., and Krakow, D. (2009). A Recessive Skeletal Dysplasia, SEMD Aggrecan Type,
732 Results from a Missense Mutation Affecting the C-Type Lectin Domain of Aggrecan. Am. J. Hum. Genet.
733 *84*, 72–79.

734 Triche, T.J., Weisenberger, D.J., Van Den Berg, D., Laird, P.W., and Siegmund, K.D. (2013). Low-level
735 processing of Illumina Infinium DNA Methylation BeadArrays. Nucleic Acids Res. *41*, e90.

736 Trinkaus, E. (2003). Neandertal faces were not long; modern human faces are short. Proc. Natl. Acad. Sci.
737 U. S. A. *100*, 8142–8145.

738 Varanasi, S.S., Olstad, O.K., Swan, D.C., Sanderson, P., Gautvik, V.T., Reppe, S., Francis, R.M., Gautvik,
739 K.M., and Datta, H.K. (2010). Skeletal site-related variation in human trabecular bone transcriptome and
740 signaling. PLoS One *5*.

741 Wagner, J.R., Busche, S., Ge, B., Kwan, T., Pastinen, T., and Blanchette, M. (2014). The relationship
742 between DNA methylation, genetic and expression inter-individual variation in untransformed human
743 fibroblasts. Genome Biol. *15*, R37.

744 Waki, H., Nakamura, M., Yamauchi, T., Wakabayashi, K. ichi, Yu, J., Hirose-Yotsuya, L., Take, K., Sun,
745 W., Iwabu, M., Okada-Iwabu, M., et al. (2011). Global mapping of cell type-specific open chromatin by
746 FAIRE-seq reveals the regulatory role of the NFI family in adipocyte differentiation. PLoS Genet. *7*.

747 Wang, H., Maurano, M.T., Qu, H., Varley, K.E., Gertz, J., Pauli, F., Lee, K., Canfield, T., Weaver, M.,
748 Sandstrom, R., et al. (2012). Widespread plasticity in CTCF occupancy linked to DNA methylation.
749 Genome Res. *22*, 1680–1688.

750 Weaver, T.D. (2009). The meaning of Neandertal skeletal morphology. Proc. Natl. Acad. Sci. *106*, 16028–
751 16033.

752 Weber, J., and Pusch, C.M. (2008). The lumbar spine in Neanderthals shows natural kyphosis. Eur. Spine
753 J. *17*.

754 Yan, Y.-L., Willoughby, J., Liu, D., Crump, J.G., Wilson, C., Miller, C.T., Singer, A., Kimmel, C.,
755 Westerfield, M., and Postlethwait, J.H. (2005). A pair of Sox: distinct and overlapping functions of
756 zebrafish sox9 co-orthologs in craniofacial and pectoral fin development. Development *132*, 1069–1083.

757 Yao, B., Wang, Q., Liu, C.F., Bhattaram, P., Li, W., Mead, T.J., Crish, J.F., and Lefebvre, V. (2015). The
758 SOX9 upstream region prone to chromosomal aberrations causing campomelic dysplasia contains multiple
759 cartilage enhancers. Nucleic Acids Res. *43*, 5394–5408.

760 Zeng, J., Konopka, G., Hunt, B.G., Preuss, T.M., Geschwind, D., and Yi, S. V. (2012). Divergent Whole-
761 Genome Methylation Maps of Human and Chimpanzee Brains Reveal Epigenetic Basis of Human
762 Regulatory Evolution. Am. J. Hum. Genet. *91*, 455–465.

763 Zilberman, U., and Smith, P. (1992). A comparison of tooth structure in Neanderthals and early Homo
764 sapiens sapiens: a radiographic study. J. Anal *180*, 387–393.

765 Ziller, M.J., Gu, H., Müller, F., Donaghey, J., Tsai, L.T.-Y., Kohlbacher, O., De Jager, P.L., Rosen, E.D.,
766 Bennett, D.A., Bernstein, B.E., et al. (2013). Charting a dynamic DNA methylation landscape of the human
767 genome. Nature *500*, 477–481.

768

769

Acknowledgements

We would like to thank Sagiv Shifman, Yoel Rak, Philip Lieberman, Rodrigo Lacruz, Erella Hovers, Anna Belfer-Cohen, Achinoam Blau, and Daniel Lieberman for their useful advice, Janet Kelso for providing data, and Maayan Harel for illustrations. L.C and E.M are supported by the Israel Science Foundation FIRST individual grant (ISF 1430/13). D.G. is supported by the Clore Israel Foundation. D.R. is an Investigator of the Howard Hughes Medical Institute and is also supported by an Allen Discovery Center for the Study of Human Brain Evolution funded the Paul G. Allen Family Foundation. S.P. and K.P. were supported by ERC grant (No 694707) and the Max Planck Society. C.L.-F. is supported by FEDER and BFU2015-64699-P grant from the Spanish government. R.P. was supported by ERC starting grant ADNABIOARC (263441). Funding for the collection and processing of the 850K chimp data was provided by the Leakey Foundation Research Grant for Doctoral Students, Wenner-Gren Foundation Dissertation Fieldwork Grant (Gr. 9310), James F. Nacey Fellowship from the Nacey Maggioncalda Foundation, International Primatological Society Research Grant, Sigma Xi Grant-in-Aid of Research, Center for Evolution and Medicine Venture Fund (ASU), Graduate Research and Support Program Grant (GPSA, ASU), and Graduate Student Research Grant (SHESC, ASU) to G.H. Collection of the chimpanzee bone from Tanzania was funded by the Jane Goodall Institute, and grants from the US National Institutes of Health (AI 058715) and National Science Foundation (IOS-1052693), and facilitated by Elizabeth Lonsdorf and Beatrice Hahn.

Tables and Figures

Table 1. DMRs in genes affecting the voice and larynx.

DMG	Associated phenotype	Chr	DMR start	DMR end
ALPL	Abnormality of the voice	1	21901961	21907487
AHDC1	Laryngomalacia	1	27869253	27871400
AHDC1	Laryngomalacia	1	27917471	27921806
SATB2	Abnormality of the voice	2	200236735	200244763
SPEG	Dysphonia	2	220316303	220319764
COLQ	Weak cry	3	15508914	15512536
TGFBR2	Abnormality of the voice	3	30649533	30658854
TGFBR2	Abnormality of the voice	3	30674279	30680742
TGFBR2	Abnormality of the voice	3	30706167	30710950
POC1A	High pitched voice	3	52110680	52112683
PLXND1	Abnormality of the voice	3	129312022	129315078
SH3BP2	Abnormality of the voice	4	2796208	2800983
SDHA	Hoarse voice, loss of voice, vocal cord paralysis	5	251676	254993
GLI3	Laryngeal cleft	7	42212811	42214593
CHD7	Abnormality of the voice, Laryngomalacia	8	61679558	61684133
COL2A1	Backwards displacement of the tongue base	12	48362098	48394211
HNRNPA1	Bowing of the vocal cords, hoarse voice	12	54679251	54682731
TRPV4	Vocal cord paresis	12	110248589	110250088
MEIS2	Laryngomalacia	15	37217518	37219852
ACAN	Hoarse voice	15	89333945	89344957
CREBBP	Laryngomalacia	16	3828787	3834862
CREBBP	Laryngomalacia	16	3891316	3900883
XYLT1	High-pitched voice	16	17428938	17431410
WWOX	Abnormality of the voice	16	78707061	78709972
SOX9	Laryngomalacia	17	70077734	70113643
SOX9	Laryngomalacia	17	70119247	70120418
GNAL	Laryngeal dystonia	18	11747116	11748993
NFIX	Laryngomalacia	19	13155588	13158871

NFIX	Laryngomalacia	19	13185658	13192650
POLD1	High-pitched voice	19	50883926	50885758
RIN2	High-pitched voice	20	19944783	19947262
PI4KA	Difficulties in speaking, chewing, and swallowing	22	21102507	21105410

792

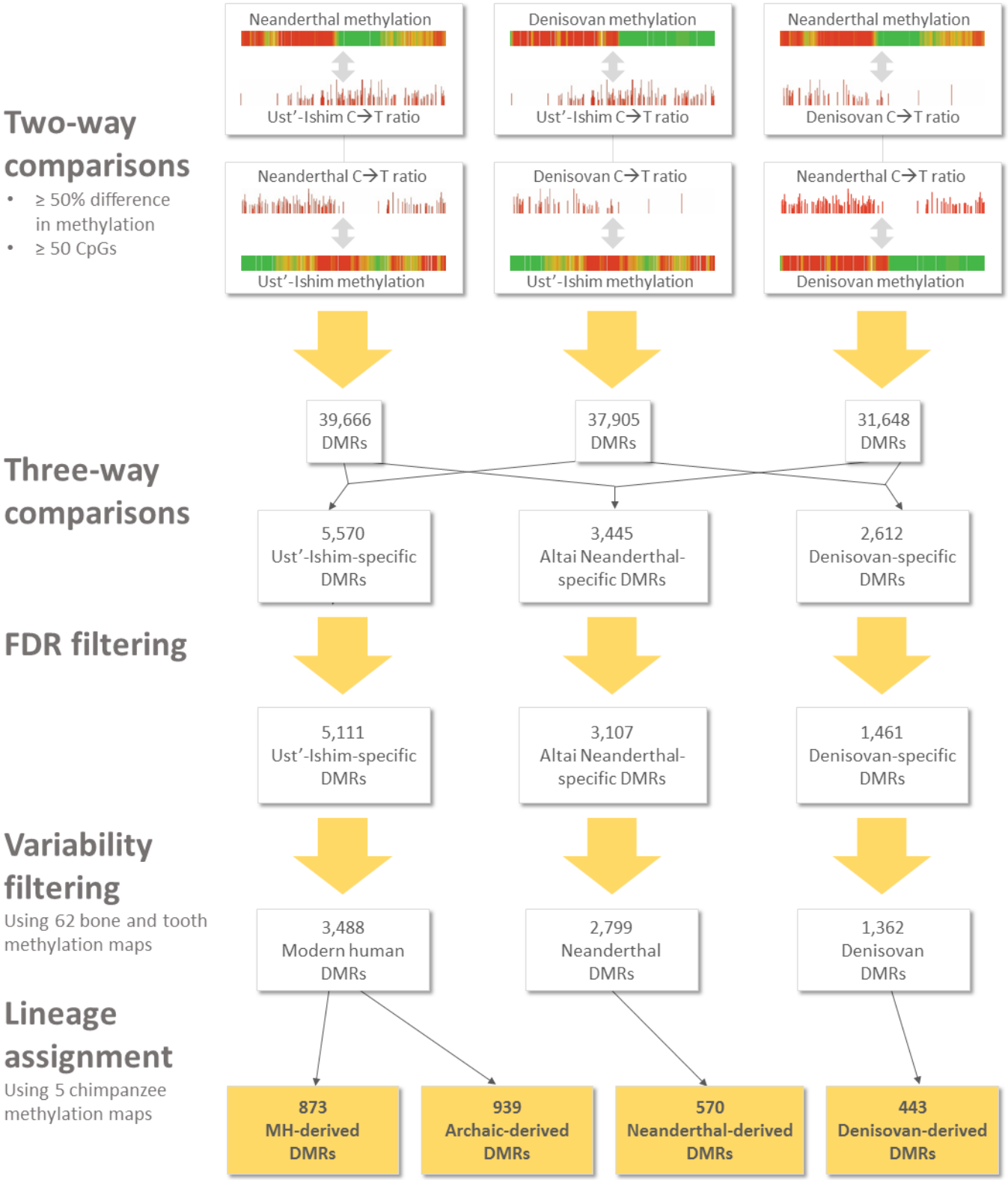

794 **Figure 1. DMR-detection flowchart.** At the core of the process are six two-way (pairwise)
795 comparisons between the Altai Neanderthal, Denisovan, and Ust'-Ishim individuals. In each two-
796 way comparison, a C→T deamination signal of one hominin was compared to the reconstructed
797 methylation map of the other hominin. This resulted in three lists of pairwise DMRs, that were
798 then intersected to identify hominin-specific DMRs, defined as DMRs that appear in two of the
799 lists. False discovery rates were controlled by running 100 simulations for each hominin, each
800 simulating the processes of deamination, methylation reconstruction, and DMR-detection. Only
801 DMRs that passed FDR thresholds of < 0.05 were kept (see Methods). To discard non-evolutionary
802 DMRs we used 62 skeletal methylation maps, and kept only loci whose methylation levels differed
803 in one lineage, regardless of age, bone type, disease or sex. Finally, five chimpanzee methylation
804 maps were used to assign the lineage in which each DMR likely emerged.

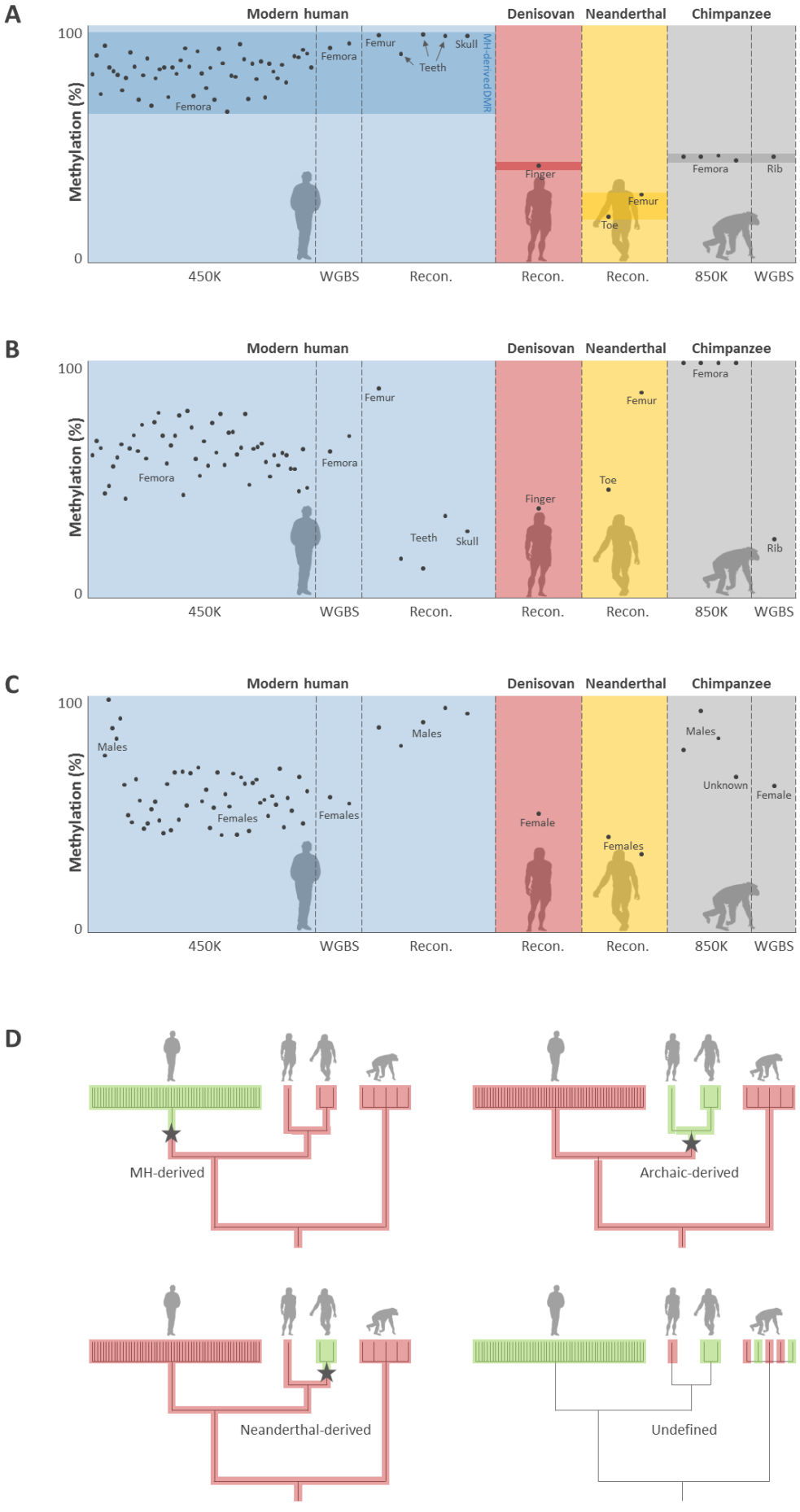

Figure 2. Variability filtering and lineage assignment. A. Methylation levels across MH, Denisovan, Neanderthal, and chimpanzee samples in DMR#278 (chr4: 38,014,896-38,016,197) located in the gene body of *TBC1D1*. This is an example of an evolutionary DMR, defined as a locus in which all 59 MH samples are found outside the range of methylation across archaic humans. RRBS samples were not used in the filtering step due to their tendency to sample unmethylated positions. Chimpanzee samples were used during the following step of lineage assignment. **B.** A putative limb-specific DMR (chr3:14,339,371-14,339,823) which was removed from the analysis, as it does not comply with our definition of evolutionary DMR. Femur, toe, and finger samples are hypermethylated compared to other skeletal elements. Toe and finger are found at the bottom range of limb samples, suggesting some variation in this locus within limb samples too. **C.** A putative sex-specific DMR (chr3:72,394,336-72,396,901) which was removed from the analysis, as it does not comply with our definition of evolutionary DMR. Males are hypermethylated compared to females. **D.** Lineage assignment using chimpanzee samples. Each bar at the tree leaves represents a sample. Methylation levels are marked with red and green, representing methylated and unmethylated samples, respectively. Only DMRs that passed the previous variability filtering steps were analyzed. The lineage where the methylation change has likely occurred (by parsimony) is marked by a star. For example, DMRs where chimpanzees cluster closer to archaic samples were defined as MH-derived.

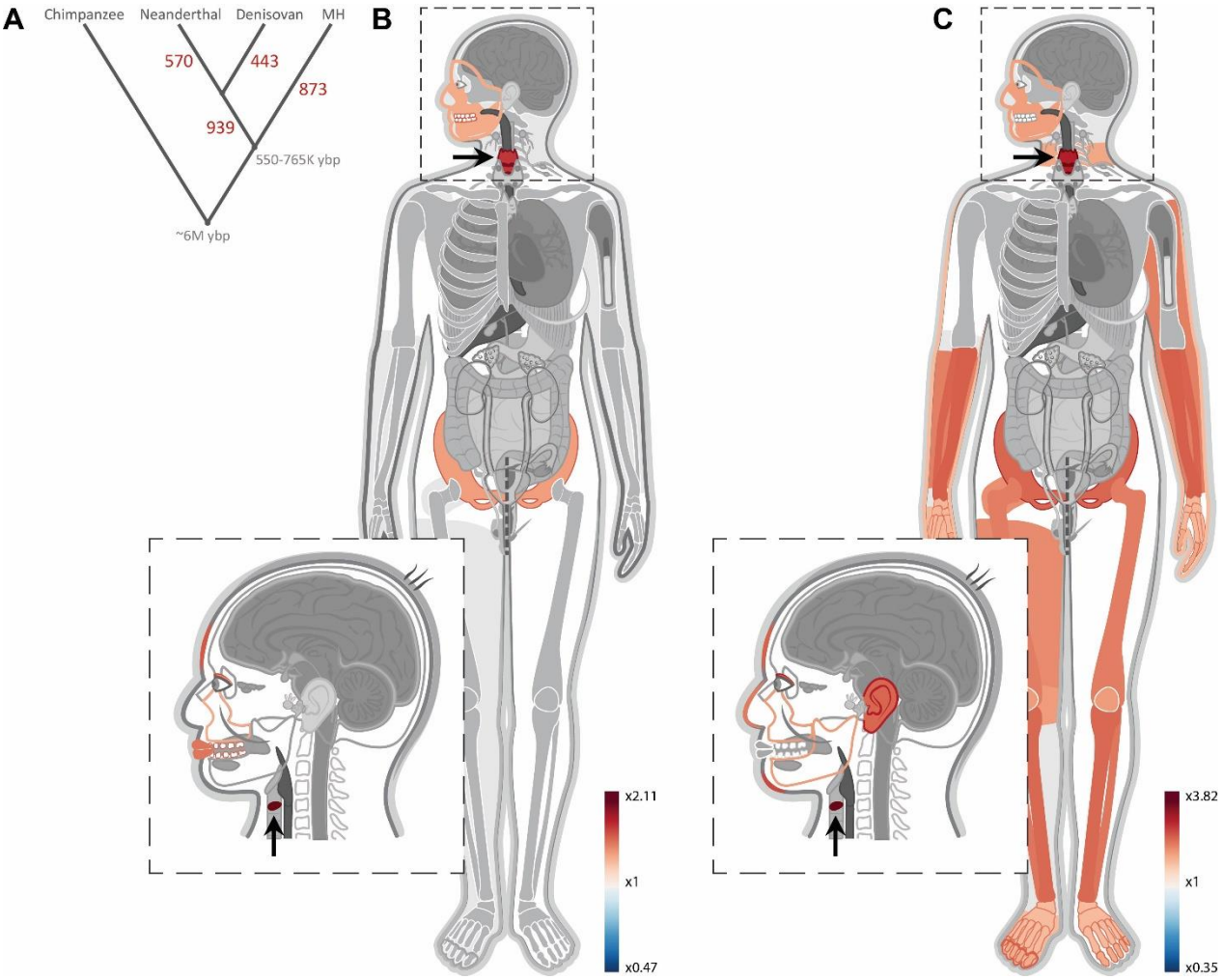

824

825 **Figure 3. Genes affecting voice and face are the most over-represented within MH-derived**
826 **DMRs. A.** The number of DMRs that emerged along each of the human branches. Split times are
827 in years before present (ybp). **B.** A heat map representing the level of enrichment of each
828 anatomical part within the MH-derived DMRs. Only body parts that are significantly enriched
829 (FDR < 0.05) are colored. Three skeletal parts are significantly over-represented: the face, pelvis,
830 and voice box (larynx, marked with arrows). **C.** Enrichment levels of anatomical parts within the
831 most significant (top quartile) MH-derived DMRs, showing a more pronounced enrichment of
832 genes affecting vocal and facial anatomy.

833

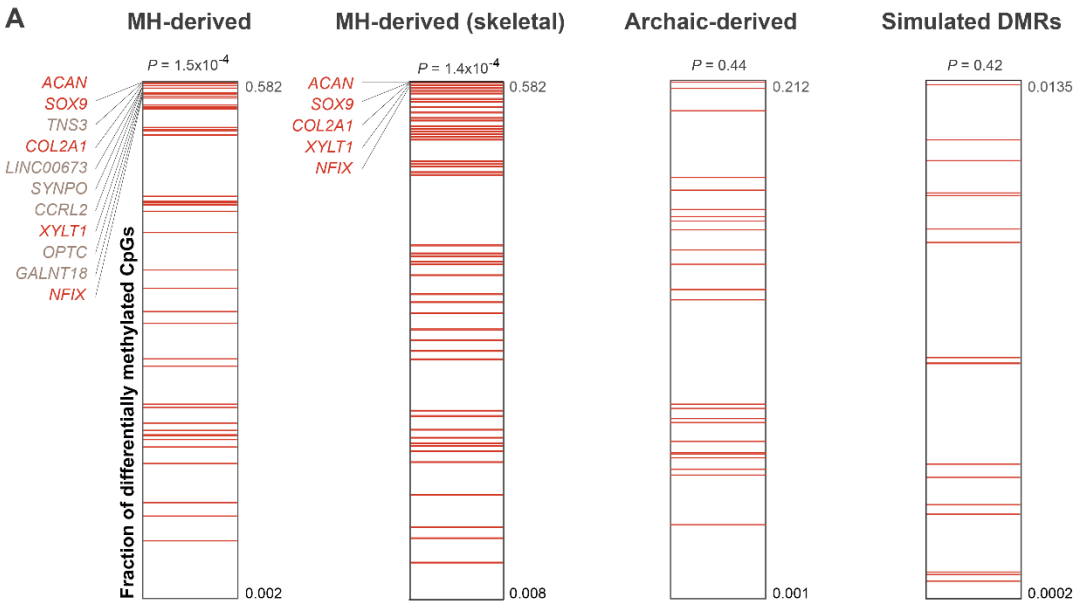

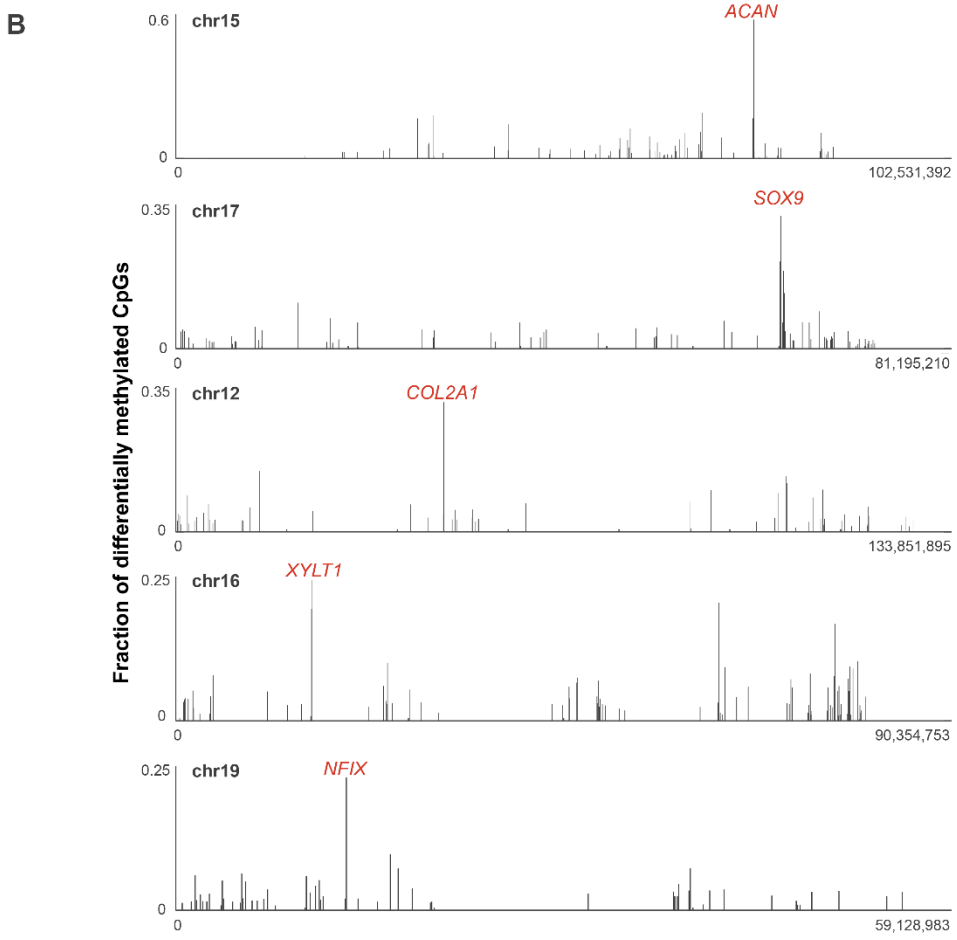

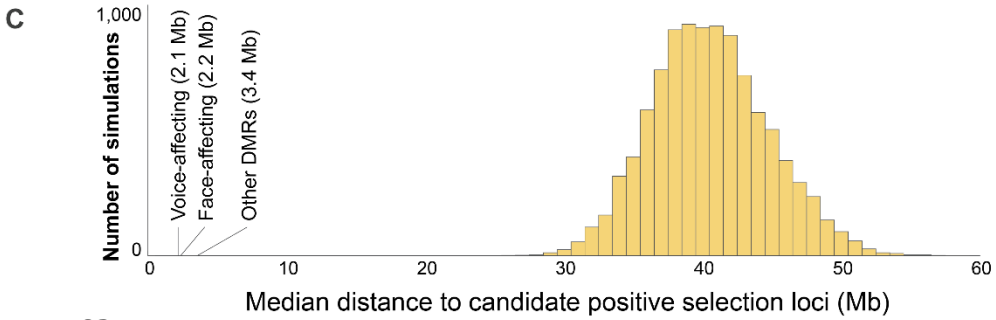

Figure 4. The extent of differential methylation is highest among genes affecting the voice. **A.** The fraction of differentially methylated CpG positions was computed as the number of MH-derived CpGs per 100 kb centered around the middle of each DMR. Genes were ranked according to the fraction of derived CpG positions within them. Genes affecting the voice are marked with red lines. MH-derived DMGs which affect the voice tend to be ranked significantly higher. Although these genes comprise less than 2% of the genome, three of the top five MH-derived DMGs, and all top five skeleton-related MH-derived DMGs affect the voice. In archaic-derived DMRs and in simulated DMRs, voice-affecting genes do not show higher ranking compared to the rest of the DMGs. **B.** The fraction of differentially methylated CpGs along the five chromosomes containing *ACAN*, *SOX9*, *COL2A1*, *XYLT1*, and *NFIX*. In each of these chromosomes, the most extensive changes are found within the genes *COL2A1*, *SOX9*, *ACAN*, and *NFIX*. All of these genes control facial projection and the development of the larynx. **C.** Mean distance of randomized DMRs to putative selective sweep regions (Peyrégne et al., 2017). Each DMR was allocated a random genomic position, while keeping its original length. This was repeated for 10,000 iterations. DMRs tend to be found significantly closer to putative selective sweep regions than expected by chance. DMRs in voice- and face-affecting genes tend to be 2x closer to such regions compared to other DMRs.

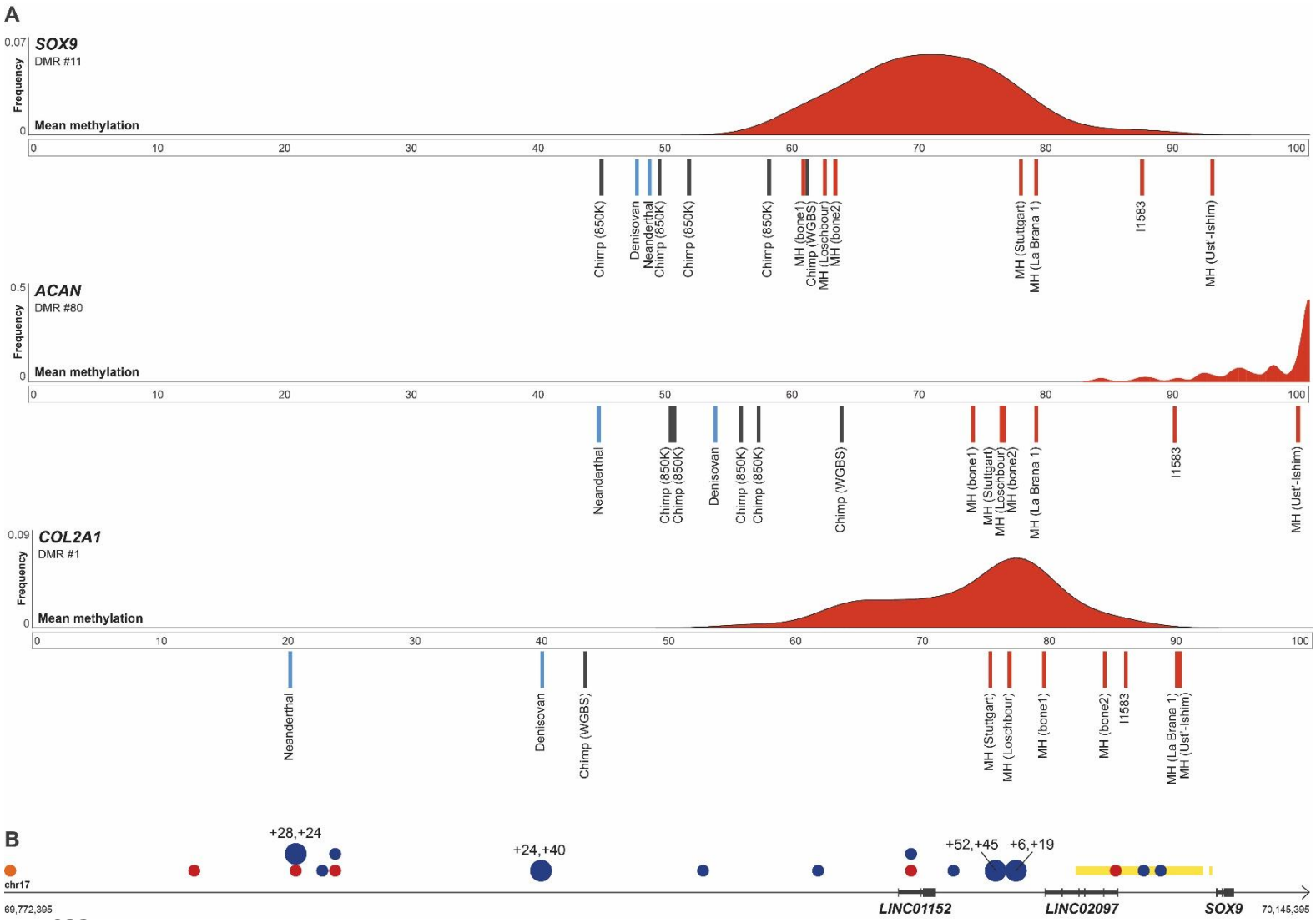

854 **Figure 5. Hypermethylation of *SOX9*, *ACAN*, and *COL2A1* in MHs. A.** Methylation levels in
855 the MH-derived DMRs in *SOX9*, *ACAN*, and *COL2A1*. MH samples are marked with red lines,
856 archaic human samples are marked with blue lines and chimpanzee samples are marked with grey
857 lines. The distribution of methylation across 52 MH samples (450K methylation arrays) is
858 presented as a red distribution. **B.** *SOX9* and its upstream regulatory elements. MH-derived DMRs
859 are marked with yellow rectangles, enhancers identified in humans are marked with red dots, and
860 enhancers identified in mice are marked with blue dots. Enhancers which were shown to be active
861 in skeletal tissues (mainly cartilage) are marked with large dots, and a putative enhancer that bears

862 active histone marks in chimpanzee, but not in modern humans is marked with an orange dot.
863 Numbers above skeletal enhancers show the difference in mean bone methylation between MHs
864 and archaic humans (left) and between MHs and chimpanzee (right). Across all four enhancers,
865 MHs are hypermethylated compared to archaic humans and the chimpanzee.

866

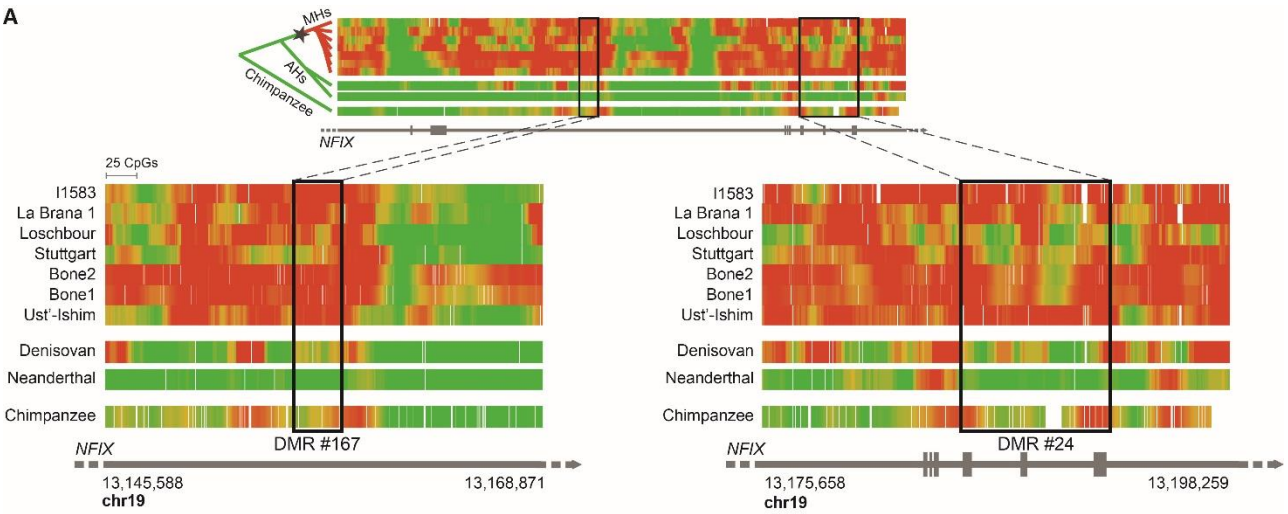

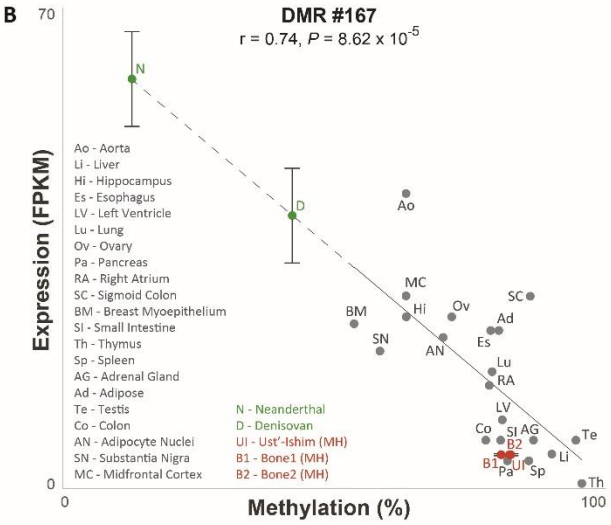

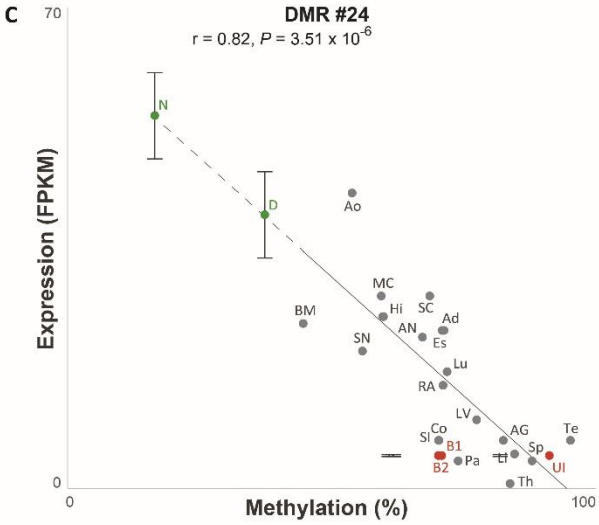

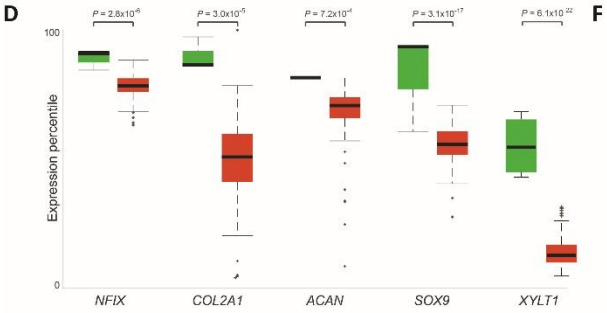

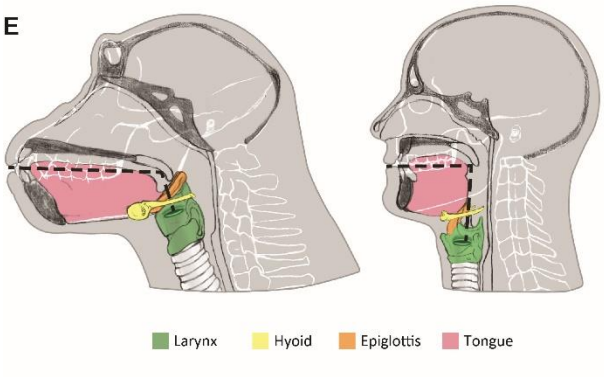

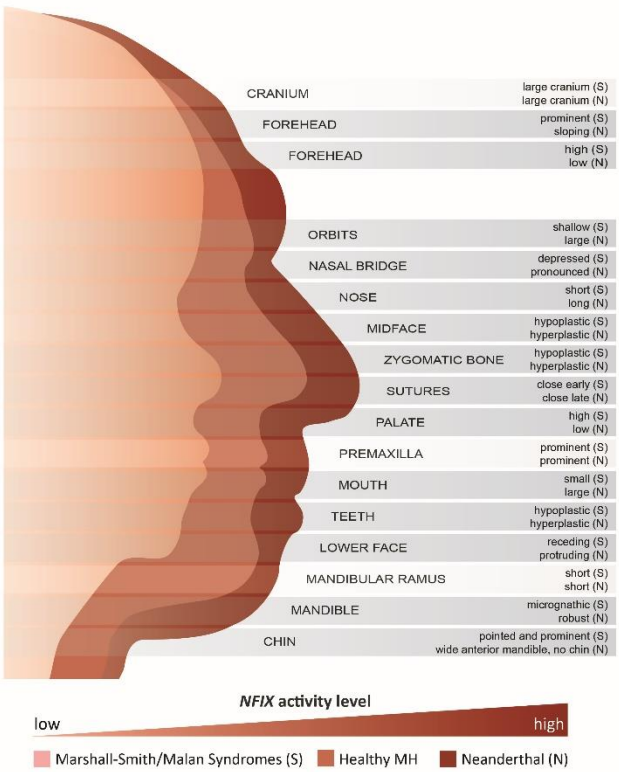

Figure 6. *NFIX* became down-regulated after the split from archaic humans. A. Methylation levels along *NFIX*, color-coded from green (unmethylated) to red (methylated). In each of the two panels, the top seven bars show ancient and present-day MH samples, where *NFIX* is mostly methylated. The bottom three maps describe the Denisovan, Neanderthal (archaic humans, AHs), and chimpanzee, where the gene is mostly unmethylated. Methylation levels around the two MH-derived DMRs (#24 and #167) are shown in the zoomed-in panels. These two DMRs represent the regions where the most significant methylation changes are observed, but hypermethylation of *NFIX* in MHs can be seen throughout the entire gene body. Chimpanzee and present-day samples were smoothed using the same sliding window as in ancient samples to allow easier comparison. The inferred schematic regulatory evolution of *NFIX* is shown using a phylogenetic tree to the left of the top panel. Star marks the shift in methylation from unmethylated (green) to methylated (red). **B,C**. Methylation levels in DMRs #167 and #24 vs. expression levels of *NFIX* across 21 MH tissues (grey). In both DMRs, higher methylation is associated with lower expression of *NFIX*. Ust'-Ishim, Bone1 and Bone2 methylation levels (red) are plotted against mean NFIX expression from four present-day bones. Neanderthal and Denisovan methylation levels (green) are plotted against the predicted expression levels, based on the extrapolated regression line (dashed). Error bars represent one standard deviation in each direction. **D.** Expression levels of *SOX9*, *ACAN*, *COL2A1* and *NFIX* in modern humans are reduced compared to mice. The box plots present 89 human samples (red) and four mouse samples (green) from appendicular bones (limbs and pelvis). Expression levels were converted to percentiles, based on the level of gene expression compared to the rest of the genome in each sample. **E.** Vocal anatomy of chimpanzee and MH. The vocal tract is the cavity from the lips to the larynx (marked by dashed lines). In MHs, the flattening of the face together with the descent of the larynx led to approximately 1:1 proportions of the

horizontal and vertical portions of the vocal tract, whereas chimpanzees have a longer horizontal and a shorter vertical vocal tract. **F**. Craniofacial features of the Neanderthal (posterior silhouette), healthy MH (middle silhouette), and MH with Marshall-Smith or Malan syndromes (anterior silhouette). *NFIX* controls the upper vs. lower prognathism of the face. Individuals where *NFIX* is partially or completely inactive present phenotypes that are largely the opposite of the Neanderthal facial features. For each facial part we show the phenotype of the Marshall-Smith and Malan syndromes (S), as well as the corresponding Neanderthal (N) phenotype. Phenotypes are compared to a healthy MH. Opposite phenotypes are marked with dark grey rectangles, and shared phenotypes are marked with light grey rectangles.

Supplementary Figures

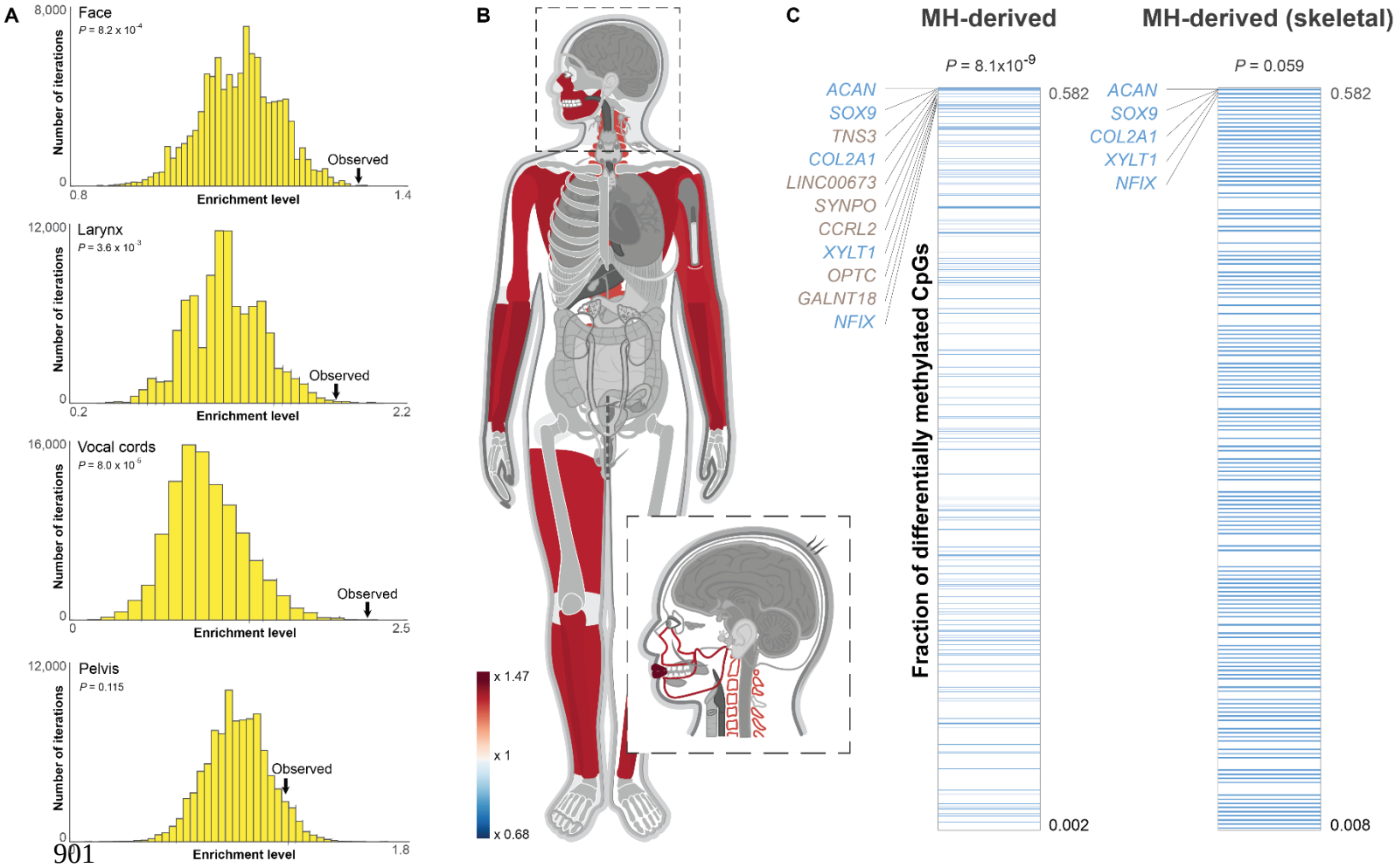

Figure S1. The face and larynx are enriched within MH-derived DMGs compared to genes affecting the skeleton, and compared to archaic-derived DMGs. A. The distribution of enrichment levels in 100,000 randomized lists of genes, where non-skeletal MH-derived DMGs were unchanged, whereas skeleton-related DMGs were replaced with random skeleton-related genes. Observed enrichment levels are significantly higher than expected in the face, larynx, and vocal cords. **B.** A heat map representing the level of enrichment of each anatomical part within archaic-derived DMGs. Genes affecting the lips, limbs, jaws, scapula, and spinal column are the most enriched within archaic-derived DMRs. Only body parts that are significantly enriched

(FDR < 0.05) are colored. **C.** The number of MH-derived CpGs per 100 kb centered around the middle of each DMR. Genes were ranked according to the fraction of derived CpG positions within them. Genes affecting the face are marked with blue lines. MH-derived DMGs which affect the face tend to be ranked significantly higher. Although only ~2% of genes in the genome are known to affect lower and midfacial projection, three of the top five MH-derived DMGs, and all top five MH-derived skeleton-affecting DMGs affect facial projection.

A

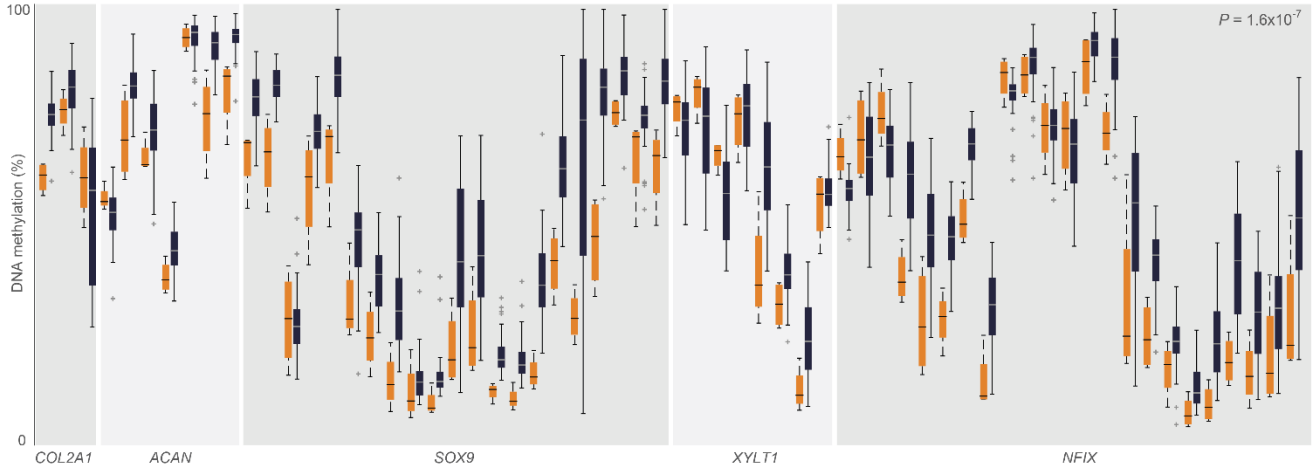

B

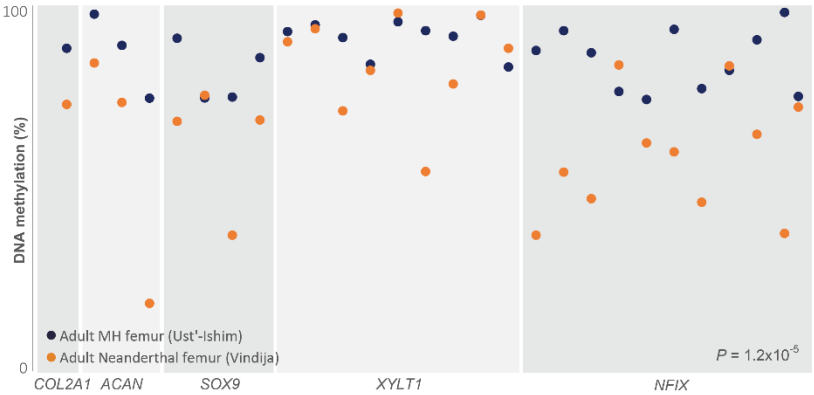

C

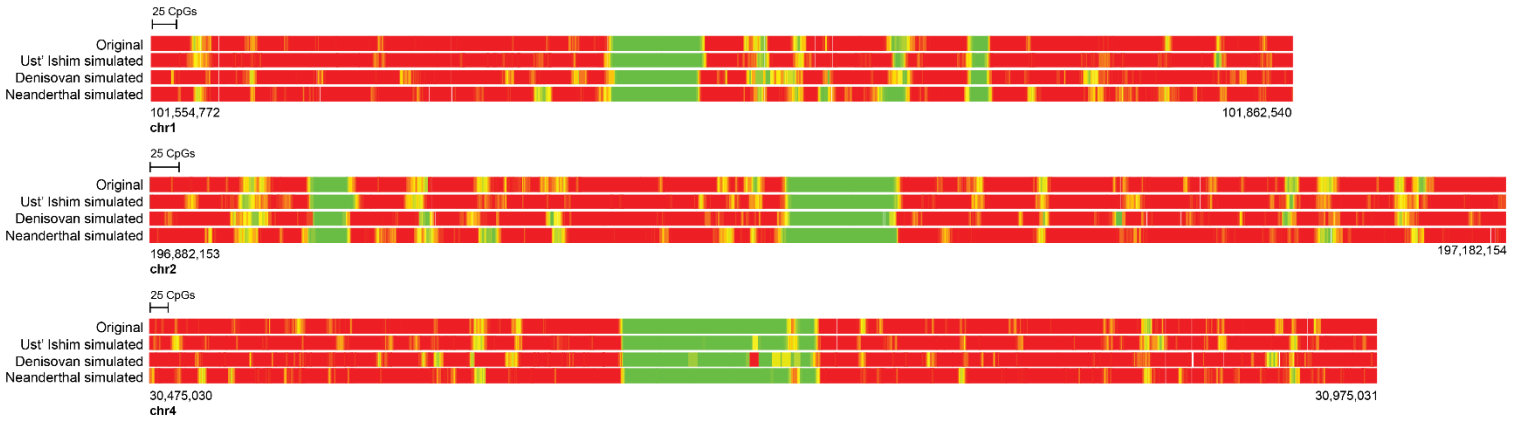

D

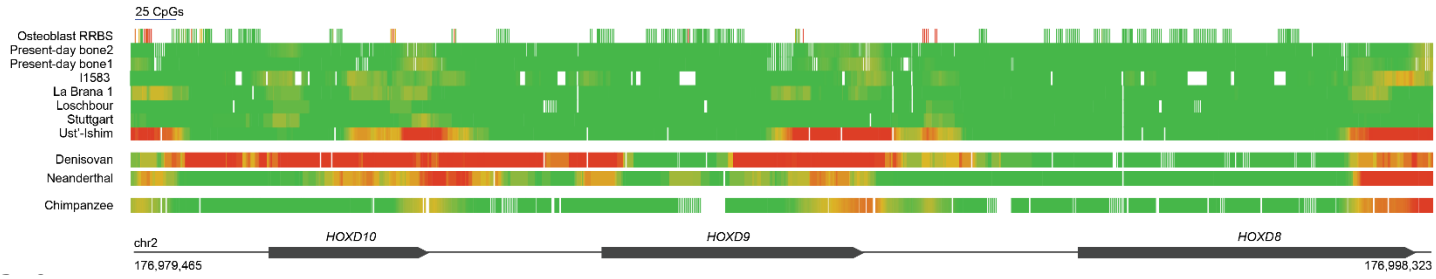

Figure S2. A. *COL2A1, ACAN, SOX9,* and *NFIX* are hypermethylated in MH femora compared to chimpanzee femora. Each pair of box plots represents methylation levels across 52 MH femora (blue) and four chimpanzee femora (orange) in a single probe of methylation array. When comparing methylation in the same bone, measured by the same technology, and across the same positions, MHs show almost consistent hypermethylation compared to chimpanzee. The probes presented include also probes within DMRs that were analyzed in the density analyses (see Methods). **B.** *COL2A1, ACAN, SOX9,* and *NFIX* are hypermethylated in Ust'-Ishim (blue) compared to the Vindija Neanderthal (orange). Dots represent mean methylation levels in MH-derived DMRs. Both samples were extracted from femora of adults, and methylation was reconstructed using the same method. The DMRs presented include also those that were analyzed in the density analyses (see Methods). The hypermethylation of these genes in MHs is unlikely to be attributed to age or bone type. **C.** Simulations of cytosine deamination, followed by reconstruction reproduce DNA methylation maps. Deamination was simulated for each position based on its methylation level, read coverage and the observed rate of deamination in each hominin. Then, DNA methylation maps were reconstructed and matched against the original map. The number of DMRs found were used as an estimate of false discovery rate. Three exemplary regions are presented, where methylation levels are color-coded from green (unmethylated) to red (methylated). **D.** The HOXD cluster is hypermethylated in archaic humans, and in the Ust'-Ishim individual. Methylation levels are color-coded from green (unmethylated) to red (methylated). The top eight bars show ancient and present-day MH samples, the lower three show the Denisovan, Neanderthal and chimpanzee. The promoter region of *HOXD9* is hypermethylated in the Neanderthal and the Denisovan, but not in MHs. The 3' ends of the three genes are

939 hypermethylated in the Neanderthal, Denisovan, Ust'-Ishim and chimpanzee, but not in other MH

940 samples. The promoter of HOXD10 is methylated only in the Denisovan.

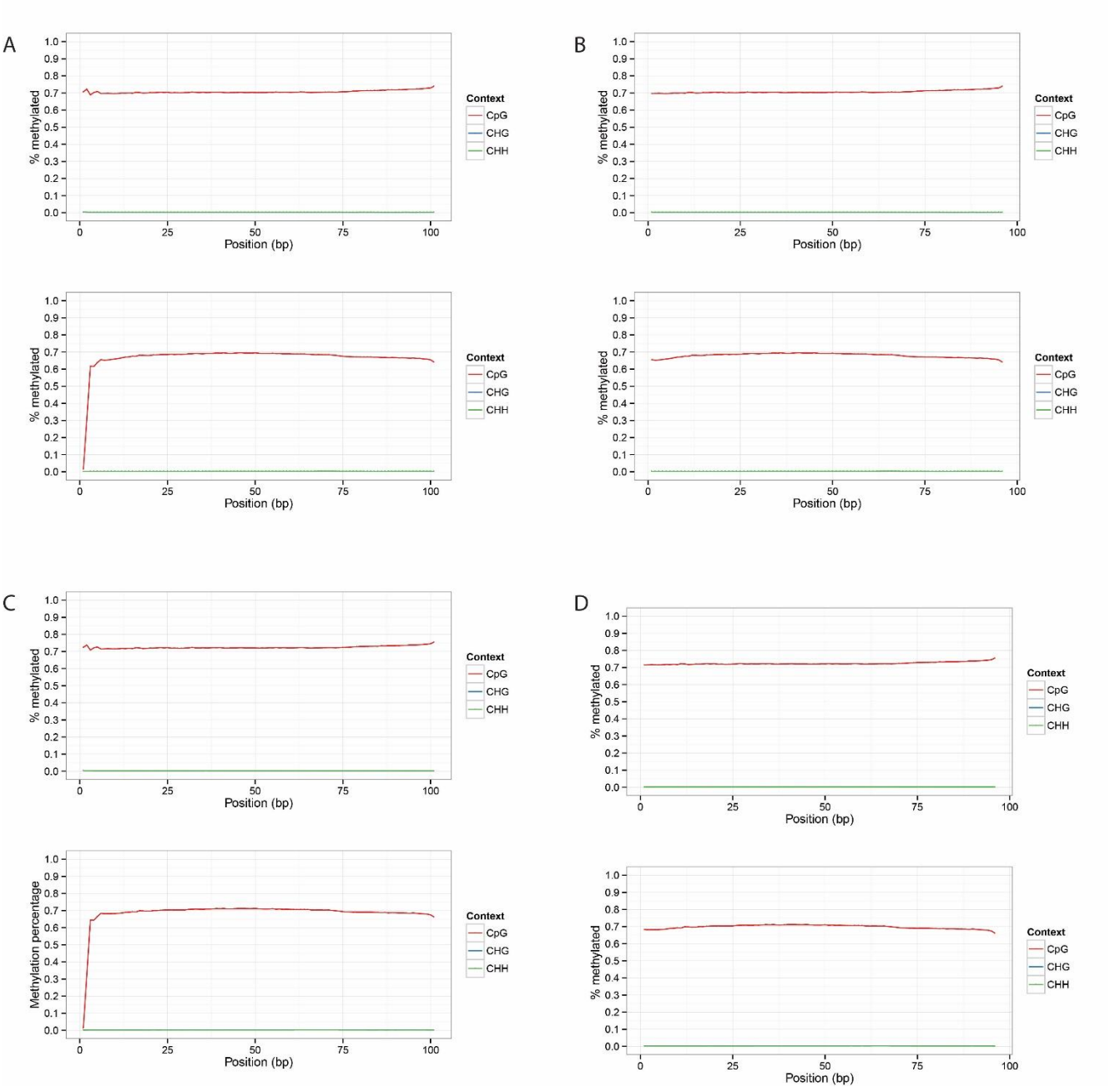

941

942 **Figure S3**. **M-bias plots along reads in bone sample 1 and sample 2**. **A**. Pre-filtering
943 methylation along read1 and read2 in the autosomes of bone 1. **B**. Post-filtering methylation along
944 read1 and read2 in the autosomes of bone 1. **C**. Pre-filtering methylation along read1 and read2 in
945 the autosomes of bone 2. **D**. Post-filtering methylation along read1 and read2 in the autosomes of
946 bone 2.

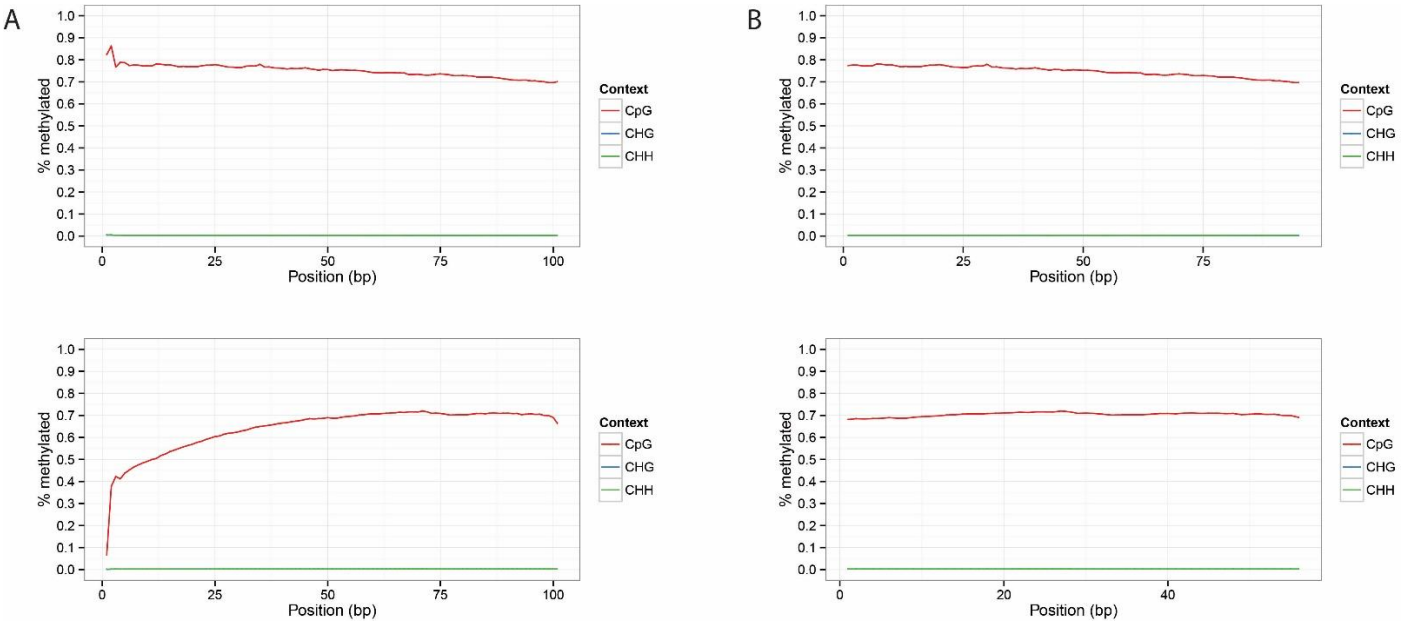

947

948 **Figure S4**. **M-bias plots along reads in the chimpanzee rib sample**. **A**. Pre-filtering methylation

949 along read1 and read2 in the autosomes. **B**. Post-filtering methylation along read1 and read2 in the

950 autosomes.